Contract No.:

This manuscript has been authored by Savannah River Nuclear Solutions (SRNS), LLC under Contract No. DE-AC09-08SR22470 with the U.S. Department of Energy (DOE) Office of Environmental Management (EM).

Development of the hybrid sulfur cycle for use with concentrated solar heat input

Highlights

- Design options evaluated for hybrid sulfur cycle water-splitting using solar heat
- Indirect solar heating with thermal energy storage using falling particle receiver
- Continuous operation with liquid-fed electrolyzer, bayonet acid decomposer
- Detailed flowsheet with material and energy balances prepared and presented
- 35.0% LHV cycle efficiency, 17.0% solar-to-H_2 conversion ratio estimated

Development of the hybrid sulfur cycle for use with concentrated solar heat. I. Conceptual design

Claudio Corgnale[a], Maximilian B. Gorensek[b,*], and William A. Summers[a]

[a]*Savannah River Consulting, LLC, 301 Gateway Drive, Aiken, SC 29803 USA*
[b]*Strategic Development and Innovation, Savannah River National Laboratory, Building 703-41A, Aiken, SC 29808 USA*

Abstract

A detailed conceptual design of a solar hybrid sulfur (HyS) cycle is proposed. Numerous design tradeoffs, including process operating conditions and strategies, methods of integration with solar energy sources, and solar design options were considered. A baseline design was selected, and process flowsheets were developed. Pinch analyses were performed to establish the limiting energy efficiency. Detailed material and energy balances were completed, and a full stream table prepared. Design assumptions include use of: location in the southwest US desert, falling particle concentrated solar receiver, indirect heat transfer via pressurized helium, continuous operation with thermal energy storage, liquid-fed electrolyzer with PBI membrane, and bayonet-type acid decomposer. Thermochemical cycle efficiency for the HyS process was estimated to be 35.0%, LHV basis. The solar-to-hydrogen (STH) energy conversion ratio was 16.9%. This exceeds the Year 2015 DOE STCH target of STH > 10%, and shows promise for meeting the Year 2020 target of 20%.

Keywords: hybrid sulfur cycle; concentrated solar; falling particle receiver; thermal energy storage; conceptual design

* Corresponding author. Tel.: (803) 725-1314; E-mail address: maximilian.gorensek@srnl.doe.gov

Acronyms

BPVE	Biphenyl vinyl ether
DLR	Deutsches Zentrum für Luft- und Raumfahrt
DOE	(United States) Department of Energy
EERE	(Office of) Energy Efficiency and Renewable Energy
FCTO	Fuel Cell Technology Office
FPR	Falling Particle Receiver
HEN	Heat exchanger network
HyS	Hybrid sulfur
LHV	Lower heating value
MSE	Mixed-solvent electrolyte
MYRDD	Multi-year Research, Development, and Demonstration (plan)
NHI	Nuclear Hydrogen Initiative
NRTL	Non-random two-liquid
PBI	Polybenzimidazole
PEM	Proton exchange membrane (a.k.a. polymer electrolyte membrane)
PFCB	Perfluorocyclobutyl
SDAPP	Sulfonated Diels-Alder polyphenylene
SDE	SO_2-depolarized electrolyzer
SNL	Sandia National Laboratories
SOL2HY2	Solar to Hydrogen Hybrid Cycles
SRNL	Savannah River National Laboratory
STCH	Solar Thermochemical Hydrogen (program)
STH	Solar-to-hydrogen
TES	Thermal energy storage
USC	University of South Carolina

1

1. Introduction

Using sunlight to make hydrogen by splitting water has been the subject of much interest over the past few decades since it holds the promise of a limitless clean energy source. A variety of approaches has been proposed and investigated, including photoelectrochemical, electrolytic, and thermochemical methods. One of the most advanced of the thermochemical water-splitting methods is the hybrid sulfur (HyS) cycle (Figure **1**), originally proposed over forty years ago by Brecher and Wu [1] at Westinghouse Electric Corp.. Known also as the Westinghouse (or Westinghouse sulfur) cycle because of its origins, HyS is considered a hybrid thermochemical cycle because it includes an electrolytic step, the SO_2-depolarized electrolysis of water, which makes sulfuric acid at the anode and hydrogen at the cathode at only a small fraction of the standard potential for water electrolysis. The cycle is completed with just one additional reaction, the high-temperature decomposition of sulfuric acid into water, SO_2, and oxygen.

HyS is the only practical two-step thermochemical cycle with all fluid reactants, which greatly simplifies material handling and processing and reduces capital costs. Various aspects of HyS are the subject of active research internationally as indicated by a quick gleaning of the literature since 2015 [2-19]. Both reaction steps have been experimentally validated [16, 20] and detailed system designs have been proposed for continuous, steady-state applications [21, 22]. However, terrestrial sunlight is not continuous, but varies diurnally as well as seasonally, and is unavailable at least half of the time. That means the design of a terrestrial HyS process driven by a solar heat source has to accommodate the cyclic nature of the primary energy source. This can be done in any of three ways:

- Design the process to run only when there is sufficient sunlight;

- Design those parts of the process that rely on solar heat to run intermittently, providing enough intermediate product (chemical) storage capacity to allow the rest of the plant to operate continuously using grid power; or
- Provide enough high-temperature heat storage capacity to allow the entire process to run continuously.

The first (and simplest) option, intermittent operation seems obvious. However, this would require an instantaneous production capacity about three times larger than the average production rate since the process will be idle more than half of the time. Furthermore, daily heating up and cooling down of process equipment would introduce thermal stresses that could shorten component lifetimes. The other two options offer some relief from these drawbacks, but at the cost of additional complexity.

Guerra Niehoff et al. [23] chose the second alternative when they proposed a solar HyS process with a sulfuric acid decomposition section that operates diurnally while the rest of the process runs continually. Their approach relies on large storage tanks to accumulate and dispense three intermediate streams for integrated operation. Kolb et al. [24] opted for the third alternative, proposing a solar HyS process that operates continually, storing high-temperature heat to allow sulfuric acid decomposition throughout the day. Their approach requires a solar receiver with a large thermal energy storage (TES) system. As these two examples demonstrate, the choice involves trade-offs between the cost and practicality of chemical versus heat storage.

Another design decision is whether to apply solar heat directly to the high-temperature process units, or indirectly using a heat-transfer medium. Obviously, if a TES system is being used indirect heating is the only choice. However, direct heating of the sulfuric acid vaporizer and high-temperature decomposition reactor is possible with the chemical storage option. For

example, Guerra Niehoff et al.'s design places both the vaporizer and reactor at the focal point of a solar concentrator [23]. While direct heating is inherently simpler, the resulting extreme diurnal temperature swings as well as the shorter transients due to cloud cover raise concerns about thermal fatigue in components that handle highly corrosive fluids. (Thermal fatigue is a known issue in the design of liquid central receivers for concentrating solar power [25].) Direct heating of the vaporizer also limits opportunities for recuperative evaporation, which is needed to overcome the latent heat energy penalty.

Other design decisions include solar receiver type and whether to use an SO_2-depolarized electrolyzer (SDE) with a vapor- or liquid-fed anode. All of these choices will ultimately impact the performance and the cost of the solar HyS plant.

This paper presents the conceptual design of a solar HyS process developed for the Solar Thermochemical Hydrogen (STCH) program under DOE's Office of Energy Efficiency and Renewable Energy (DOE-EERE) Fuel Cell Technology Office (FCTO) sponsorship. A follow-on paper will provide a techno-economic analysis of a 50-MT/d implementation of this process as well as a path forward to solar HyS production at \$2/kg H_2, the ultimate goal of the STCH program.

2. Flowsheet alternatives

The design of the solar HyS process flowsheet began by considering all possible configurations to ensure the best possible outcome. This led to evaluation and comparison of four basic sets of alternatives: 1) liquid- versus vapor-fed SDE; 2) direct versus indirect (i.e., using an intermediate heat transfer fluid) solar heating of process units; 3) thermal versus chemical energy storage (to allow continuous hydrogen production); and 4) solar receiver types. These are considered in the following subsections.

2.1.Liquid- versus vapor-fed SDE

Practical considerations dictate that the SDE needs to produce sulfuric acid at the highest possible concentration to minimize the amount of water that has to be removed before the acid is sent to the high-temperature decomposition reactor. Excess water imposes an energy penalty, so an acid concentration in excess of 50 wt% is desired. This requirement rules out Nafion® as a viable proton exchange membrane (PEM) candidate, since its resistivity increases rapidly as H_2SO_4 concentration approaches 50 wt% due to membrane dehydration [26]. Consequently, the design assumed that an advanced membrane would be used instead. Several advanced SDE membranes are being considered for HyS, including a sulfonated Diels-Alder polyphenylene (SDAPP) membrane made by Sandia National Laboratories (SNL) [27] and a sulfonated perfluorocyclobutyl (PFCB) biphenyl vinyl ether block copolymer (BPVE-6F) provided by Clemson University and Tetramer Technologies [28], but for design analysis purposes an H_2SO_4-doped polybenzimidazole (PBI) membrane being developed at the University of South Carolina (USC) [19] was selected. The reason for this choice is that the PBI membrane can operate at high temperatures (160°C and higher) and its resistivity is not adversely affected by high sulfuric acid concentrations. (Higher temperature operation of the SDE should result in a lower overpotential due to faster kinetics and mass transfer rates. USC has recently shown good SDE performance – 0.66 V at 0.5 A/cm^2 – with PBI membranes operating at 120°C and producing sulfuric acid at 8 mol/L H_2SO_4 concentration [29].) A key implication of this assumption, however, is that the cathode side of the PEM cannot be exposed to a water stream, because the acid dopant would be leached out. Consequently, the SDE had to be configured with the anode side exposed to sulfuric acid and a dry cathode. This is different than previous SDE work which included a Nafion® membrane and a water saturated cathode [22].

Two different SDE designs were considered. One had liquid anolyte (SO_2 dissolved in sulfuric acid) and no catholyte feed streams, with liquid anolyte (sulfuric acid product) and gaseous catholyte (hydrogen) product streams. The liquid anolyte configuration is similar to the one used by SRNL in its prior HyS cycle development work for the DOE Nuclear Hydrogen Initiative (NHI) [22]. The other design approach shared the same cathode configuration, but assumed a gaseous anode feed (SO_2 vapor saturated with water at its vapor pressure) and the anode effluent was a two-phase mixture containing primarily unreacted SO_2 vapor and liquid sulfuric acid. This configuration is being used at USC to test H_2SO_4-doped PBI membranes [19].

Flowsheets were prepared for both SDE configurations. The target H_2SO_4 concentration was set at 65 wt% and the target hydrogen pressure at 300 psig (21.7 bar abs). It soon became apparent that the liquid anolyte-fed alternative was the better choice, in particular for PEMs that require a dry cathode. There are several reasons why.

First, the gaseous anolyte feed composition is limited by the vapor pressure of water. At 5 bar and 125°C, the SO_2 vapor feed becomes saturated with water vapor at about 47 mol% H_2O. If the total pressure is doubled to 10 bar, the water vapor saturation content drops to 24 mol%. Since almost three moles of water enter the product unconverted for every two moles that react with SO_2 to form 65 wt% sulfuric acid, less than half of the water vapor in the feed stream is actually available for the electrochemical reaction. Furthermore, two moles of H_2O are required for each mole of SO_2 reacted. Consequently, the vapor-fed SDE configuration is limited to operation at relatively low pressures, and the per-pass SO_2 conversion is limited to relatively small fractions. A large vapor recycle stream is needed and the product hydrogen stream has to be compressed to 300 psig, imposing an additional energy penalty.

Second, vapor-fed operation of the SDE is complicated by the presence of two phases in the anode space. The design of the anode has to let fresh vapor feed reach every corner while allowing acid product to form within the porous gas diffusion layer and be collected for withdrawal as product. This requires a more complex, and potentially more costly design than that for a liquid-fed SDE.

Third, the vapor-fed SDE involves reactants in the vapor phase combining to form a liquid product. Condensation in any form will release latent heat. That means the SDE has to be cooled not only to remove the heat generated due to cell overpotentials, but to remove the heat released by condensation of the vapor phase reactants into a liquid product as well. The heat duty is overwhelming, amounting to about 2½ times the equivalent electric power input to the SDE at 600 mV cell potential. Consequently, a vapor-fed SDE would need to be built with internal circulation of a coolant for heat removal and temperature control, greatly increasing the complexity and cost. It should be noted that this limitation applies only to vapor-fed SDEs that have a dry cathode. If water could be circulated through the cathode (not an option for acid-doped PBI membranes), cell temperature could be controlled by means of the sensible heat of the recirculating water stream.

Finally, the SDE coolant would need to be able to transfer some of the heat removed from the SDE to the feed vaporizers for the overall process to be practical from the standpoint of energy efficiency. Given the small temperature differences involved and the likely small heat transfer coefficient on the hot side, the resulting vaporizers would have impractically large heat transfer areas.

For these reasons, the baseline flowsheet was assumed to use a liquid-fed SDE with a dry cathode.

2.2.Direct versus indirect solar heating

Two options were considered for solar heat input to the process. Both options assume concentrated solar energy using a heliostat field and a tower with a solar receiver. The first option was to apply concentrated solar heat directly to the high-temperature units in the process that require heat input by locating them in the receiver aperture. Those units are the sulfuric acid vaporizer and the high-temperature decomposition reactor. The German Aerospace Agency (Deutsches Zentrum für Luft- und Raumfahrt, or DLR) is developing prototypes of these units at their Jülich Solar Tower Research Facility for the European SOL2HY2 (Solar to Hydrogen Hybrid Cycles) project [7, 9]. The other option was to use the solar concentrator to heat a high-temperature heat transfer fluid instead, using a heat exchanger network to distribute the heat to the process as needed. Although to the authors' knowledge no one is currently developing hardware for this specific purpose, conceptual designs were prepared based on hardware being developed for solar electric power generation.

Flowsheets were prepared for both options. Based on previous experience with the HyS cycle under the NHI, a bayonet configuration was chosen for the sulfuric acid decomposition reactor in the indirect solar heat input flowsheet. The bayonet design allows for a moderate temperature liquid feed, a moderate temperature two-phase vapor/liquid product, and internal recuperation. This keeps the high-temperature heat requirement for sulfuric acid decomposition at a minimum and facilitates component construction and choice of materials. When the solar heat input requirements for flowsheets using an indirectly heated bayonet reactor were compared with those of flowsheets utilizing a directly heated vaporizer and decomposition reactor like DLR's, the latter were found to require substantially more heat input, making them significantly less energy efficient. The reason for this is that a substantial portion of the heat requirement for

sulfuric acid vaporization is provided by internal recuperation in the bayonet, while all of the heat input for the directly heated vaporizer comes from the sun. DLR's current prototypes are also limited to atmospheric pressure operation, whereas a pressurized acid decomposition system is preferred to reduce equipment size and cost and to better integrate with the balance of the process.

Based on these considerations, indirect solar heating using a high-pressure helium heat transfer fluid was chosen for the baseline flowsheet.

2.3. Thermal versus chemical energy storage

Concentrated solar heat is available only about one-third of the time, taking the diurnal cycle and weather conditions into account. Consequently, a solar HyS process cannot generate hydrogen continuously, unless there is some provision for temporary energy storage that can be tapped when solar heating is not available. The principal advantage of continuous operation is size and the resultant capital cost: the same daily production capacity can be achieved by a continuous plant one-third the size of an intermittent plant that runs only when the sun is shining.

Two options were considered for energy storage. The obvious, but technically more challenging one is high-temperature (> 900°C) thermal storage. If high-temperature heat could be stored for 16 hours or more (in the form of a heat transfer medium), then the plant could be operated continuously. In that case, the solar heat input would be indirect by definition. The other option is chemical energy storage in the form of concentrated sulfuric acid produced by the SDE on a continuous basis, and in the form of the SO_2/water product of high-temperature sulfuric acid decomposition produced intermittently during times of solar operation. This entails splitting the process into a diurnal and a continuous section that can be operated independently. The logical split would be between diurnal (intermittent) operation of the acid decomposition

section, which requires high-temperature heat input, and continuous operation of the SDE, which can draw electricity from the grid. Chemical energy storage of sufficient capacity would allow independent operation of these two sections. Since the high-temperature section of the plant would be operated intermittently, it would need to be oversized by approximately a factor of three compared to the electrolysis section.

2.4. Solar receiver types

Three different solar receiver designs were considered. The first was DLR's direct solar heated evaporator and high-temperature decomposition reactor [7, 9]. In this design, both the acid vaporizer and decomposition reactor are in a tower located at the focal point of the heliostat field. Operation is limited to periods of insolation, making it necessary to use chemical energy storage to allow the SDE to run 24 h/d. For reasons elaborated in section 2.2, this option was eliminated from further consideration for the baseline design. However, should DLR develop a design capable of operating at greater than atmospheric pressure and with internal recuperation, this could be a strong alternative.

The second solar receiver design considered was SNL's Falling Particle Receiver (FPR) [30]. This is also a concentrated solar heat design that uses a field of heliostats to direct solar radiation to a receiver in a tower. The FPR draws sand-like particles from a low-temperature storage tank; passes them in a falling curtain through the focal point of the heliostat field, heating them up to a temperature in excess of 800°C; and stores them in another, high-temperature storage tank. The two insulated tanks or reservoirs are sized to capture the maximum daily total heat input from the sun. Hot particles are continually drawn from the high-temperature reservoir, used to heat an appropriate heat transfer fluid (like supercritical CO_2 or pressurized helium), and returned to the low-temperature reservoir. Cooled particles are removed from the low-

temperature reservoir during times of adequate solar radiation and conveyed to the top to the tower where they pass through the receiver once again. The heat transfer fluid can then be used for heat input to a continuous HyS process. (Sandia is developing the FPR for continuous electric power generation under a research program for the DOE SunShot Initiative [31].) This is a way to achieve TES and to permit continuous HyS system operation. A prototype of the FPR is currently undergoing testing at Sandia [32].

A third solar receiver concept was considered as a back-up. This design was developed by Brayton Energy, LLC under the SunShot Initiative for power generation [33]. The receiver features a novel extended area heat exchanger behind a quartz window at the focal point of the heliostat field that heats supercritical CO_2 to temperatures in excess of 750°C. This concept could be modified to heat pressurized helium to higher temperatures, allowing intermittent operation of the decomposition reaction section of the HyS process with chemical energy storage.

Based on these considerations, the FPR approach with a pressurized helium secondary heat transfer fluid was selected for the baseline flowsheet.

3. Baseline solar HyS cycle process flowsheet

The baseline flowsheet for the solar HyS process features a liquid-fed SDE operating at 22 bar and 120°C that produces 65-wt% H_2SO_4 at a 50%-per-pass conversion and 600-mV cell potential. TES in the form of an FPR solar collector with a pressurized helium secondary heat transfer loop allows continuous operation of the entire HyS process plant. Acid decomposition takes place in a bayonet reactor heated to a peak process fluid temperature of 850°C at a feed pressure of 14 bar. Aspen Plus™ was utilized to simulate the process and generate material and energy balances. This flowsheet is described below. Feed preparation and utilities as well as

product purification are assumed to use the same operations as those described in [34], and so are not detailed here.

A new physical properties model was developed for this work. It uses the symmetric electrolyte-NRTL model for the H_2SO_4-H_2O-SO_3 system developed by Que et al. [35] modified to include SO_2. Previously published work (e.g., [21, 22, 36-38]) made use of the OLI-MSE (mixed-solvent electrolyte) model [39] for characterizing phase equilibria and calculating liquid phase properties. However, dew point calculations for sulfuric acid solutions using the OLI-MSE model often didn't converge or gave erratic results. Furthermore, since the purely vapor phase equilibrium between SO_3 and SO_2 in the decomposition reactor at high temperatures is based on a hypothetical liquid phase oxidation-reduction reaction involving HSO_4^- and SO_2 in the OLI-MSE model, we chose to use an equation-of-state model with Aspen Plus™ RGibbs free energy minimization for the SO_3 decomposition reaction instead. This necessitated a switch between properties models at the points of transition to and from all-vapor flow and introduced a discontinuity in the sulfuric acid vaporization and condensation calculations. Finally, using the OLI Engine in Aspen Plus™ was found to increase computation time by an order of magnitude or more. Consequently, we chose to use a new properties model that does not have these shortcomings and can be used over the entire flowsheet. A paper describing the new, symmetric electrolyte-NRTL model is being submitted for publication [40].

3.1. SO_2-depolarized electrolysis section

The SO_2-depolarized electrolysis section of the solar HyS cycle flowsheet is shown in Figure **2**. The associated stream table is presented as Table **1**. The flowsheet has been scaled to a hydrogen/SO_2 production rate of 1 kmol/s for convenient scaling to any other production rate.

Fresh water (stream 1) and the wet SO_2 (stream 56) and sulfurous acid (stream 75) products of acid decomposition are pressurized to 22.7 bar, added to the anolyte recycle (stream 32), and fed to the SDE anode (stream 3). No water is fed to the cathode side of the SDE as discussed previously in section 2.1. SO_2-depolarized electrolysis in electrolyzer EL-01 is assumed to take place at a cell potential of 600 mV and to result in half of the SO_2 entering with stream 3 being oxidized to H_2SO_4, producing an equimolar quantity of hydrogen. Hydrogen product exits via stream 4 at 130°C and 21.7 bar, while spent anolyte exits via stream 5 at the same temperature and pressure. A pressure drop of 1 bar is assumed for flow through the anode, and the overpotential results in an anolyte temperature increase of about 15°C.

Splitter SP-01 draws off a product stream carrying 1 kmol/s of H_2SO_4 (stream 6) and recycles the rest of the spent anolyte (stream 29). The pressure of the product stream is dropped adiabatically to atmospheric via throttling valve VV-01 to flash off dissolved SO_2 in vapor/liquid separator (knock-out pot) KO-01. The pressure of the remaining liquid (stream 8) is dropped once again in throttling valve VV-02 to a vacuum (0.1075 bar) to flash off more dissolved SO_2 in knock-out KO-02. The acid product of SO_2-depolarized electrolysis containing 65 wt% H_2SO_4 (stream 11/12) is pumped to the acid decomposition section (or storage in TK-01) at atmospheric pressure by pump PP-02.

Vapor from the first knock-out (stream 13) is cooled to 40°C by heat exchanger HX-01 and sent to knock-out KO-03, which separates the condensate (stream 22) containing primarily water from the remaining SO_2-rich vapor (stream 15). The SO_2-rich vapor is compressed to 21.2 bar in a three-stage compressor (CO-01) with intercooling, and condensed by cooling to 40°C in heat exchanger HX-02. The resulting liquid (stream 17) is added to the spent anolyte recycle stream in stream mixer MX-01.

Vapor from the second knock-out (stream 18) is cooled to 40°C by heat exchanger HX-03 and sent to knock-out KO-04, which separates the condensate (stream 20) containing most of the water from the remaining vapor (stream 24) containing most of the SO_2. Condensate is pressurized to atmospheric pressure and forwarded to knock-out KO-03. The vapor is compressed to atmospheric pressure in a two-stage compressor (CO-01) with an intercooler, and condensed by cooling to 40°C in heat exchanger HX-05. The resulting liquid (stream 26) is fed to knock-out KO-03. Intercooler condensate (stream 27) is pressurized to atmospheric pressure by pump PP-05 and also fed to knock-out KO-03. The liquid collected in KO-03 (stream 22) is pressurized to 21 bar and added to the spent anolyte recycle stream in stream mixer MX-01.

Heat generated due to the overpotential in EL-01 is recovered in heat exchanger HX-04, which cools the anolyte recycle stream to a temperature low enough to maintain a 130°C outlet temperature (using a design-spec in Aspen Plus™). The anolyte recycle rate is controlled by another design-spec to ensure that it is sufficient to keep 2 kmol/s of SO_2 dissolved at SDE feed conditions (about 2,350 kg/s spent anolyte). Recycled anolyte is pressurized back up to 22.7 bar by pump PP-06 and fed to the SDE.

3.2. High-temperature H_2SO_4 decomposition section

The high-temperature H_2SO_4 decomposition section of the solar HyS cycle flowsheet is shown in Figure **3**. The associated stream table is presented as **Table 2**. The flowsheet has been scaled to a hydrogen/SO_2 production rate of 1 kmol/s for convenient scaling to any other production rate.

65 wt% sulfuric acid (stream 12) is fed to a vacuum column (TO-01) operating at an overhead pressure of 0.1 bar. The column has four equilibrium stages including a reboiler and total condenser, with a pressure drop of 0.015 bar from bottoms to overhead. Four stages were

found to be adequate for the task of concentrating sulfuric acid. The (nearly pure water) distillate rate is set to give a bottoms product (stream 35) with roughly 90 wt% H_2SO_4 content.

The concentrated sulfuric acid is pressurized to 12.5 bar pressure and fed to a quench column (TO-02), where it contacts the effluent from the decomposition reactor. This column has only two equilibrium stages, one of which is the partial condenser, and a negligible pressure drop. It serves to trap any unconverted H_2SO_4 from the decomposition reactor so that it can be recycled with the bottoms. The bottoms (stream 37) are pressurized to 14.1 bar pressure and fed to the bayonet reactor (RX-01), which is assumed to have a pressure drop of 1 bar. Bayonet reactor product (stream 39) is cooled to 260°C and fed back to the quench column.

The bayonet reactor is heated with hot helium (875°C) generated by heat exchange with sand from the hot reservoir of the FPR. Hot helium is assumed to be available on a continuous basis. The reactor is assumed to have a 0.15-bar pressure drop in the annular boiling region, a 0.05-bar drop in the annular superheating region, a 0.5-bar drop in the annular catalyst bed, a 0.1-bar drop in the product vapor cooling region, and a 0.2-bar drop in the product condensing region, for a total pressure loss of 1 bar. Feed enters the annular region of the bayonet at 278.9°C, is completely vaporized when it reaches 446.1°C, enters the catalyst bed at 650°C, exits the catalyst at 850°C, begins to condense at 410.1°C, and exits the bayonet at 288.9°C. Since the pinch point is at the reactor exit, as determined by a pinch analysis (Section 3.4), all of the heat released by product condensation within the bayonet can be used to vaporize the feed, resulting in a high-temperature heat duty of 352.6 MW_{th}.

The overhead of the quench column is cooled to 214°C with a total liquid reflux and total vapor distillate (stream 41). Vapor distillate is cooled to 40°C in heat exchanger HX-07,

condensing most of the water and about half of the SO_2. The vapor is separated from the liquid in knock-out KO-05 and sent to the SO_2 absorber, TO-03, via stream 43.

The SO_2 absorber, which separates oxygen from SO_2 based on its different water solubility, has 10 equilibrium stages with no reboiler or condenser. (Ten stages were found to be enough to make an overhead oxygen product with ≤ 1 ppm O_2.) It operates at an overhead pressure of 11.8 bar with a 0.2-bar pressure drop from bottoms to overhead. Nearly all of the SO_2 entering the absorber exits with the water in the bottoms, while 99.7% of the oxygen exits with the overhead. The bottoms (stream 44) has its pressure dropped from 12 bar to near-atmospheric by throttling valve VV-04, is heated by interchange with the bottoms from the SO_2 stripper (TO-04) in heat exchanger HX-08, and is then fed to the fourth stage of TO-04.

The SO_2 stripper has seven equilibrium stages, including a partial vapor condenser and reboiler. It strips SO_2 from the water solvent so that the water can be recycled and reused in the absorber. (Seven stages were found sufficient to strip 99.98% of the dissolved SO_2 and essentially all of the oxygen.) The pressure drop from bottoms to overhead is assumed to be 0.15 bar. The molar reflux ratio is set at 1.5, and the molar distillate-to-feed ratio is carefully adjusted so that all of the oxygen and nearly all of the SO_2 exit with the overhead (stream 47).

The SO_2 recovered by the stripper (stream 47) is compressed to 3.687 bar by compressor CO-03, cooled to 40°C and partially condensed by heat exchanger HX-09. Its condensate is removed in knock-out KO-06 and the remaining vapor (stream 50) further compressed to 12.311 bar by compressor CO-04, after which it is cooled to 60°C by heat exchanger HX-10 and nearly completely condensed. The oxygen carried along in stream 52 is removed in the O_2 stripper (TO-05). This column is assumed to have 10 equilibrium stages, including the partial vapor condenser and reboiler. Stream 52 is fed on the sixth stage. A molar distillate-to-feed ratio of

0.009 ensures that all but a trace of the oxygen is stripped and recycled to the SO_2 absorber while leaving 99.5% of the SO_2 in the bottoms product (stream 53). The molar reflux ratio is set at 3.2. SO_2 product is cooled to 40°C by heat exchanger HX-11 and pressurized to 12 bar by pump PP-11 in preparation for passing on to the SO_2-depolarized electrolysis section (stream 56).

The overhead from the SO_2 absorber (stream 57) contains less than 1 ppm SO_2, but is saturated with water vapor at 11.8 bar and 40°C. It is passed through an O_2 dryer (DR-01) that is assumed to remove the moisture (as well as the trace of SO_2), which is then recycled to TO-03 via stream 59 by means of pump PP-12. Pure oxygen co-product exits the process through stream 58 at 11 bar and 40°C.

A small amount of make-up water (stream 61) is pumped (pump PP-13) in to the absorber/stripper water solvent loop. It replaces water lost with the SO_2 stripper overhead (stream 47), which is only partially offset by water entering the loop at the SO_2 absorber with streams 43 and 81. The bulk of the water solvent comes from the SO_2 stripper bottoms (stream 64). It is moved by pump PP-14 through the hot side of heat exchanger HX-08, to preheat the stripper feed by interchange, and through heat exchanger HX-12 to cool it further to 40°C, before it is combined with the make-up water and the water recovered by the SO_2 dryer in stream mixer MX-03 and fed to the top of TO-03 (stream 63).

Returning to the first knock-out following the quench column (KO-05), the condensate (stream 68), which is more than 75% water on a molar basis, is passed through a throttling valve (VV-05). This lowers the pressure to 3.487 bar, lowering the temperature to 23.2°C and vaporizing some of the SO_2 and a little water. The SO_2-rich vapor that remains is removed by knock-out KO-07 and sent to compressor CO-04 via stream 70. The condensate (stream 71) is dropped in pressure to atmospheric by throttling valve VV-06, further cooling it to 3.3°C and

vaporizing more SO_2 and a little more water. To avoid issues with ice formation, it is combined with water recovered from the vacuum column overhead (stream 80) in knock-out KO-08, raising the temperature to 26.2°C. What remains in the liquid phase is mostly water (stream 73), which is pressurized to 2 bar by pump PP-15 in preparation for passing on to the SO_2-depolarized electrolysis section (stream 75) as the dilute sulfurous acid feed.

The SO_2-rich vapor phase (stream 76) is recycled to compressor CO-03. The liquid phase from KO-06 (stream 77) is primarily SO_2. It is pressurized to 12 bar by pump PP-16 and combined with stream 55 to form stream 56, which is the wet SO_2 feed to the SO_2-depolarized electrolysis section. Stream 79 is the vacuum column overhead, which is maintained by vacuum pump PP-17 at 0.1 bar, discharging to atmospheric pressure via stream 80. Stream 81 is the O_2 stripper overhead, which is routed directly to the bottom stage of the SO_2 absorber.

3.3. Solar HyS flowsheet model results

Power requirements for the SDE, compressors, and pumps are presented in Table **3**. The biggest power consumer by far is the SDE, which draws 115.8 kJ/mol hydrogen product, or 115.8 MW_e at a hydrogen production rate of 1 kmol/s. The flowsheet model assumes that the SDE operates with a cell potential of 600 mV, the development target for DOE-sponsored HyS R&D. Compressors and pumps add another 10.5 MW_e, bringing the total power requirement to 126.3 MW_e.

Heating requirements for the bayonet reactor, SO_2 stripper feed/bottoms interchanger, and three reboilers are summarized in Table **4**. More than half of the 607.8-MW_{th} total duty is for the bayonet reactor, RX-01, which requires 352.6 kJ/mol SO_2 product, or 352.6 MW_{th} to sustain a hydrogen production rate of 1 kmol/s. This value was determined by a pinch analysis, following the methodology described in earlier publications [22, 37], and explained below.

Composite feed heating and product cooling curves for a bayonet reactor operating at a 1-kmol/s hydrogen production rate were extracted from the Aspen Plus™ model. These are shown in Figure **4**. The pinch point is at the reactor entrance (to the annular region) on the cold side and at the exit (from the central region) on the hot side, the coolest points on both curves. This means all of the heat rejected from the hot side can be exchanged with the cold side. The horizontal gap of 352.6 MW_{th} between the two curves at 850°C represents the heating target, which is the minimum amount of heat that needs to be provided by an external hot utility. For the solar HyS process, the hot utility is the helium heat transfer fluid. The utility and grand composite curves (Figure **5**) show that the 352.6-MW_{th} heating target can be satisfied by heat exchange with a helium heat transfer fluid supplied at a temperature of 875°C and returned at a temperature no lower than 400°C. This assumes a minimum temperature difference of 25°C between the external helium and internal process fluids and 10°C between the feed (annular) and product (central) regions. The solar HyS flowsheet model assumes that the bayonet reactor can be designed to operate at the minimum heating target.

The next biggest heating requirement is for the vacuum column reboiler at 148.4 MW_{th}, followed by the SO_2 stripper reboiler at 65.55 MW_{th}. Most of these needs can be satisfied by recuperation as will be shown in Section 3.4 below. The 40.59-MW_{th} heating requirement for the hot side of the SO_2 stripper feed/bottoms interchanger, HX-08 is already satisfied by a matching cooling requirement for the cold side (see Table **5**). Finally, the O_2 stripper reboiler requires a small amount (600 kW_{th}) of low grade (<100°C) heat that should be satisfied by recuperation as well.

Cooling requirements for the solar HyS cycle process flowsheet are summarized in Table **5**. The biggest cooling need (nearly one-fourth of the 449.9-MW_{th} total duty) is for the vacuum

column condenser, which can only reject heat to the environment due to its low temperature (46°C). The next two biggest requirements are for the quench column overhead cooler, HX-07 (95.4 MW_{th}) and the anolyte recycle cooler, HX-04 (66.7 MW_{th}). Both reject heat at temperatures that should allow recuperation. Several other cooling requirements also provide opportunities for recuperative heating, e.g., the cold side of intercooler HX-08, the bayonet reactor effluent cooler (HX-06), and the quench column (TO-02) condenser. Heat integration to maximize energy utilization is considered next.

3.4. Solar HyS cycle process flowsheet pinch analysis

A pinch analysis was performed (using Aspen Plus™ flowsheet model results imported into Aspen Energy Analyzer) to establish the limiting performance (energy efficiency) of the HyS process. This analysis is for a 1-kmol/s hydrogen/SO_2 production rate and a minimum temperature difference of 10°C (between the hot and cold streams in a heat exchanger). Note that 10°C is the default value for the minimum temperature difference for heat transfer used in Aspen Energy Analyzer. In practice, the optimal value should actually be determined for each heat exchanger individually with the objective of minimizing capital cost, but will likely not be much bigger or smaller. The composite heating and cooling curves for the HyS flowsheet are shown in Figure **6**. (The bayonet reactor is excluded from this analysis because it is considered separately from the rest of the flowsheet.) The process pinch occurs at 108.5°C on the hot composite cooling curve (hot pinch point) and 98.5°C on the cold composite heating curve (cold pinch point). The minimum heating target is 34.6 MW_{th}, and the minimum cooling target 242.7 MW_{th}. Looking to identify the heat flows which dominate the curves near the pinch, the nearly horizontal segment of the cold curve just below 100°C is contributed almost entirely by the SO_2 stripper (TO-04) reboiler, while the shallow slope segment of the hot curve between 110 and

130°C is due to the contribution of the acid recycle stream cooler (HX-04). Heat exchange between the TO-04 reboiler and HX-04, which have large duties over relatively narrow temperature ranges, determines the pinch point. Lowering the bottoms temperature in TO-04 would obviously decrease the heating target, but that could only be achieved by lowering the pressure in the column. However, since the temperature of the overhead in TO-04 (39.6°C) is already slightly below 40°C, the lower limit attainable with cooling water, further reduction would introduce the need for a chiller to cool the TO-04 condenser, which the authors have chosen to avoid. Consequently, the resulting heating and cooling targets of 34.6 and 242.7 MW_{th}, respectively, are close to the minima for this particular flowsheet for a 1-kmol/s hydrogen production rate.

The heating needs for this flowsheet could be provided by a medium-pressure (MP) steam source (condensing between 175 and 174°C) and a low-pressure (LP) steam source (condensing between 125 and 124°C), and the cooling needs by a cooling water source (operating between 29.5 and 35°C). This is shown in Figure **7**, which plots the utility and grand composite curves for the 1-kmol/s H_2 solar HyS process flowsheet. Most (27.7 MW_{th}) of the 34.6-MW_{th} heating target can be supplied by LP steam, leaving the MP steam requirement at only 6.9 MW_{th}.

As an alternative, heat could be provided directly by the hot helium heat transfer fluid exiting the bayonet reactor at 400°C. At the heating target of 34.6-MW_{th}, this would lower the helium temperature by less than 50°C, from 400 to 353.4°C, which could be easily accommodated by designing the helium heat transfer loop accordingly. Figure **8** depicts the utility and grand composite curves for this case.

4. Baseline HyS cycle process with solar heat source

As noted in Section 3, an FPR solar collector with built-in TES and a pressurized helium secondary heat transfer loop allows the baseline flowsheet for the solar HyS process to operate continuously. This means high-temperature solar heat is applied indirectly to the process through a heat transfer medium (helium), which has some advantages compared to direct solar heating, as described in Section 2.2, and allows the chemical plant to be located outside the solar tower at ground level. The intermediate heat transfer loop greatly simplifies the process plant design and operation. However, it adds an additional layer of complexity to the overall system, reducing its energy efficiency, and likely increasing the overall capital cost. Since the baseline solar process includes a sand-based TES system, it allows hydrogen production even at night or when the sun is obscured by clouds.

Detailed design, exergetic efficiency analysis, and cost estimation of the solar HyS plant are beyond the scope of this paper but will be provided in a follow-on publication.

4.1. Solar heat source – HyS process plant coupling

The solar heat source consists of a heliostat field that concentrates solar radiation on an FPR mounted on a solar tower. The FPR system includes sufficient high-temperature heat storage capacity to ensure continuous operation of the HyS process plant. One of the most important degrees of freedom in designing the solar heat source - HyS process plant interface is how to provide the required low-temperature heat for everything other than the bayonet reactor. Considering the results of the pinch analysis in Section 3.4, the low-temperature heat input will be to the vacuum column reboiler exclusively.

The low-temperature heating target represents about 9% of the total (high-temperature and low-temperature) minimum heat duty. Several approaches to provide the necessary low-

temperature heat have been considered. The simplest approach is to use the same heating medium (pressurized helium) to satisfy all external heating needs. An additional heat exchanger, part of the vacuum column reboiler system, would be located in series after the bayonet reactor. This allows easier solar plant management, but results in relatively low exergetic efficiency due to the large temperature difference between the hot and cold streams (as will be discussed in the follow-on paper). Another approach is to supply the necessary low temperature heat using an external steam (or high-pressure water) utility. The steam could be produced by a separate, low-temperature solar heat source, or could be acquired from a co-located power or process plant. Yet another option would be to extract useful work from the helium at high temperature to generate power and then heat the vacuum column reboiler with waste heat from co-generation. This approach is considerably more complicated and beyond the scope of this publication. (It will be analyzed in the follow-on paper.) Consequently the first and simplest approach (using pressurized helium as the only process heat utility) will be used for the baseline solar HyS cycle process.

A schematic showing how the solar heat source is coupled to the process plant is shown in Figure **9**. An intermediate (solid particle-gas) heat exchanger transfers high-temperature heat from the hot sand to a pressurized helium heat transfer fluid, which in turn heats the bayonet reactor and the vacuum column reboiler of the HyS process plant. This configuration is similar to that used for the conceptual designs of HyS processes developed for the NHI, leveraging the experience gained in that work. The chemical process plant is not part of the solar tower, but is located separately outside, at ground level, minimizing the possibility of chemical leaks or process upsets affecting solar tower operations. Two sand reservoirs comprise the TES system. The hot sand reservoir accumulates sand collected from the FPR while the sun is shining, and

stores it for use throughout the day. Sand is continuously withdrawn from the hot sand reservoir, passed through a solid particle-gas heat exchanger to heat the helium heat transfer fluid, and collected in the cold sand reservoir. The flow of particles from the FPR through the hot reservoir and the intermediate exchanger into the cold reservoir is gravity-driven, while a sand lift device is used to feed the FPR from the cold reservoir. Flow of pressurized gas in the helium heat transfer loop is driven by a circulator similar to those used in NHI conceptual designs, located at the lowest temperature point (between the vacuum column reboiler and the intermediate heat exchanger).

4.2. Solar plant energetic efficiency

A number of assumptions had to be made concerning the solar plant efficiency and performance in order to be able to estimate the overall plant energetic efficiency. These are detailed in Table **6**, while assumptions made concerning the intermediate heat transfer loop are reported in Table **7**. In particular, the plant was assumed to be located in the southwest US desert, where the incident solar radiation is least attenuated by clouds, haze, and humidity. Electric power was assumed to be provided by a solar electric steam power plant, having a heat-to-power conversion efficiency of 41.6% (per SunShot Initiative goals [41]). As a consequence, the overall solar-to-electric conversion efficiency is 20.6%, which is the product of the power conversion, receiver, thermal storage, and heliostat field efficiencies. Most of the intermediate heat transfer loop assumptions were made based on previously published work by the authors on both solar- and nuclear-driven hydrogen production processes [34, 42]. Helium was used as the heat transfer fluid due to the high (for a gas) convective heat transfer coefficients it allows and for its inertness. An operating pressure of 40 bar was assumed, representing a compromise between the high-pressure nuclear case (86-90 bar) [34] and lower operating pressures favorable

to the H_2SO_4 decomposition equilibrium. The overall pressure drop of 1.2 bar was calculated assuming a pressure drop of 0.5 bar in the helium side of the bayonet reactor, 0.04 bar in the helium side of the vacuum column reboiler and allowing another 0.65-bar drop in the helium piping and intermediate heat exchanger.

Based on the assumptions reported in Table **6** and Table **7**, and solving the material and energy balances for the equipment and streams shown in Figure **9**, the heat and power requirements of the solar plant were calculated and listed in Table **8**. The helium heat transfer loop was modeled using Aspen Plus™ with mass and energy balance results shown in Table **8**.

Cycle efficiency is generally used to characterize thermochemical cycles. It is based on the total thermal energy input plus the total electric power input divided by the thermal-to-electric energy conversion efficiency. The total heat duty for the HyS process plant may be calculated by adding together the bayonet reactor and vacuum column duties (heating targets). Consequently the thermochemical cycle efficiency, lower heating value (LHV) basis (η_{TC}) is:

$$\eta_{TC} = \frac{\dot{m}_{H_2} Q_{H_2,\,LHV}}{Q_{TC} + \frac{W_{TC}}{\eta_{PP}}} = \frac{241.8\ MW_{th}}{387.2\ MW_{th} + \frac{126.3\ MW_e}{0.416\ MW_e/MW_{th}}} = 35.0\%$$

where $\dot{m}_{H_2}$ is the molar production rate of hydrogen (1 kmol/s), $Q_{H_2,\,LHV}$ is the LHV of hydrogen (241.8 MJ/kmol), Q_{TC} is the total HyS process plant heat input (387.2 MW_{th}), W_{TC} is the HyS process plant electric power input (126.3 MW_e), and η_{PP} is the power cycle efficiency (assumed equal to 41.6% as shown in Table **6**).

Based on the DOE Multi-year Research, Development, and Demonstration (MYRDD) Plan [43], the solar-to-hydrogen (STH) energy conversion ratio is defined as the LHV of the net hydrogen produced divided by full-spectrum solar energy consumed. For systems utilizing solar energy input only, the energy consumed is calculated based on the incident irradiance over the total area of the solar collector. For hybrid systems, all additional non-solar energy sources (e.g.,

548 electricity) must be included as equivalent solar energy inputs added to the denominator of the
549 ratio. Consequently, the STH efficiency (η_{STH}) is:

$$\eta_{\mathrm{STH}} = \frac{\dot{m}_{\mathrm{H_2}} Q_{\mathrm{H_2,\,LHV}}}{Q_{\mathrm{HE}} + \frac{W_{\mathrm{TOT}}}{\eta_{\mathrm{TOT}}}} = \frac{241.8\ \mathrm{MW_{th}}}{761.3\ \mathrm{MW_{th}} + \frac{136.7\ \mathrm{MW_e}}{0.206\ \mathrm{MW_e/MW_{th}}}} = 17.0\%$$

550 where Q_{HE} is the total solar heat input to the heliostat field (761.3 $\mathrm{MW_e}$), W_{TOT} is the total
551 electric power input to the HyS solar plant (136.7 $\mathrm{MW_e}$), and η_{TOT} is the solar-to-electric
552 conversion efficiency, equal to 20.6% as shown in Table **6**.

553 While the MYRDD sets STH efficiency as a criterion for evaluating all STCH processes,
554 this number does not take into account the ability of hybrid cycles like HyS to draw a major
555 fraction of their energy input from the grid, which is primarily non-solar in origin. This means
556 HyS could benefit from situations where the cost of power purchased on the grid would be less
557 than that from a dedicated solar source. STH efficiency would be irrelevant in that case. The
558 real criterion, then, should be the cost of hydrogen produced by HyS, which will be discussed in
559 detail in the follow-on paper.

560 # 5. Summary and conclusions

561 A detailed analysis of a solar powered thermochemical process based on the HyS cycle
562 has been presented. Numerous design tradeoffs, including process operating conditions and
563 strategies, integration with solar energy sources, and solar design options, were considered. A
564 baseline design was selected, and process flowsheets (using Aspen Plus™) were developed. A
565 pinch analysis was performed (using Aspen Plus™ flowsheet model results imported into Aspen
566 Energy Analyzer) to establish the limiting performance (energy efficiency) of the HyS process.
567 Detailed material and energy balances were completed, and a full stream table is presented. The
568 baseline design was based on the following design selections:

- Concentrated solar power plant located in the southwest US desert;
- Falling particle receiver with indirect heat transfer to pressurized helium;
- Continuous operation based on thermal energy storage;
- Liquid-fed electrolyzer with PBI membrane;
- Bayonet-type acid decomposer

The estimated thermochemical cycle efficiency for the HyS process was calculated to be 35.0% (LHV basis). The STH energy conversion ratio was 17.0%. This exceeds the DOE STCH target for STH>10% for Year 2015 designs, and shows promise for meeting the Year 2020 target of 20%. A follow-on paper will address the means by which the STH efficiency could be increased, and will provide a techno-economic analysis of a 50-MT/d implementation of this process as well as a path forward to solar HyS production at \$2/kg H_2, the ultimate goal of the STCH program.

The HyS process is a promising option for solar thermochemical hydrogen production. Detailed analysis has shown that it can be effectively integrated with a concentrated solar power system to produce hydrogen at high efficiency. This is mainly a result of the relative simplicity of the cycle, which requires only two reaction steps and utilizes all-fluid streams. Continued experimental work is required to demonstrate the performance characteristics and verify the design assumptions for the two main HyS process reactors: the SDE and the acid decomposer. Specifically, operation of the SDE at the high pressure, temperature, and acid concentration specified in the flowsheet, heating of the bayonet reactor with pressurized helium and operation at the acid concentration and pressure in the flowsheet, and successful integration of both reactors in a closed loop process still need to be demonstrated. In addition, the solar HyS process can benefit by continued improvements in the solar energy portion of the plant,

specifically the FPR. Improvements in the performance of these components will allow further improvements in overall process efficiency. As more results from the experimental work are available, the process design analysis can be updated. Continued work is also required to verify the results of the tradeoff studies and to identify innovative solutions that can increase process efficiency and lower hydrogen production costs.

Acknowledgements

The authors gratefully acknowledge funding from the US Department of Energy's Fuel Cell Technology Office STCH program under the guidance of Dr. Eric Miller, Program Manager for Hydrogen Production & Delivery, and Dr. Katie Randolph, STCH Technology Manager. We also thank Prof. Chau-Chyun Chen and Ms. Harnoor Kaur from Texas Tech University for their help with the physical properties models used in the Aspen Plus™ simulations. SRNL is operated for the DOE's Office of Environmental Management (DOE-EM) by Savannah River Nuclear Solutions, LLC under contract number DE-A C09-08SR22470.

606 References
607
608 [1] Brecher LE, Wu CK. Electrolytic decomposition of water. United States of America:
609 Westinghouse Electric Corp.; 1975. p. 13.
610 [2] Corgnale C, Shimpalee S, Gorensek M, Weidner JW, Summers W. Modeling of a Bayonet
611 Reactor for Sulfuric Acid Decomposition in Thermo-Electrochemical Sulfur Based Hydrogen
612 Production Processes. ECS Transactions. 2017;75:7-15.
613 [3] Nadar A, Banerjee AM, Pai MR, Meena SS, Pai RV, Tewari R, et al. Nanostructured Fe2O3
614 dispersed on SiO2 as catalyst for high temperature sulfuric acid decomposition—Structural and
615 morphological modifications on catalytic use and relevance of Fe2O3-SiO2 interactions. Appl
616 Catal B Environ. 2017;217:154-68.
617 [4] Sattler C, Roeb M, Agrafiotis C, Thomey D. Solar hydrogen production via sulphur based
618 thermochemical water-splitting. Sol Energy. 2017.
619 [5] Lulu X, Ping Z, Songzhe C, Laijun W. Quantitative analysis of the cell voltage of SO2-
620 depolarized electrolysis in hybrid sulfur process. Nuclear Engineering and Design.
621 2016;306:203-7.
622 [6] Falch A, Badets VA, Labrugère C, Kriek RJ. Co-sputtered PtxPdyAlz thin film
623 electrocatalysts for the production of hydrogen via SO2(aq) electro-oxidation. Electrocatalysis.
624 2016;7:376-90.
625 [7] Lapp JL, Guerra-Niehoff A, Streber H-P, Thomey D, Roeb M, Sattler C. Modeling of a Solar
626 Receiver for Superheating Sulfuric Acid. Journal of Solar Energy Engineering.
627 2016;138:041013--10.
628 [8] Liberatore R, Lanchi M, Turchetti L. Hydrogen production by the solar-powered hybrid
629 sulfur process: Analysis of the integration of the CSP and chemical plants in selected scenarios.
630 In: Rajpaul V, Richter C, editors.: American Institute of Physics Inc.; 2016.
631 [9] Bayer Botero N, Thomey D, Guerra Niehoff A, Roeb M, Sattler C, Pitz-Paal R. Modelling
632 and scaling analysis of a solar reactor for sulphuric acid cracking in a hybrid sulphur cycle
633 process for thermochemical hydrogen production. International Journal of Hydrogen Energy.
634 2016;41:8008-19.
635 [10] Weidner JW. Electrolyzer performance for producing hydrogen via a solar-driven hybrid-
636 sulfur process. Journal of Applied Electrochemistry. 2016:1-11.
637 [11] Cichon PJ, Krüger AJ, Krieg HM, Bessarabov D, Aniol K, Kerres J. Sulfonated
638 poly(arylene thioether phosphine oxide)s and poly(arylene ether phosphine oxide)s PBI-blend
639 membranes and their performance in SO2 electrolysis. International Journal of Hydrogen
640 Energy. 2016;41:4521-37.
641 [12] Colón-Mercado HR, Corgnale C, Elvington MC, Gorensek MB, Summers WA.
642 Development of the hybrid sulfur cycle for use with concentrated solar heat input. Spanish
643 Hydrogen Association - Asociacion Espanola del Hidrogeno, AEH2; 2016. p. 421-2.
644 [13] Niehoff AG, Thomey D, Gonzales MAR, Streber HP, Lapp J, Roeb M, et al.
645 Thermodynamic model of a solar receiver for superheating of sulfur trioxide and steam at pilot
646 plant scale. American Society of Mechanical Engineers; 2016.
647 [14] Xue L, Zhang P, Chen S, Wang L. In-situ electrochemical impedance spectroscopy
648 measurement of anodic reaction in SO2 depolarized electrolysis process. Chem Eng Process:
649 Process Intensif. 2015;89:70-4.
650 [15] Turchetti L, Liberatore R, Sau S, Tizzoni AC. Carbon-free production of hydrogen via the
651 solar powered hybrid sulfur cycle: The SOL2HY2 project. In: Pierucci S, Klemes JJ, editors.

652 Chemical Engineering Transactions: Italian Association of Chemical Engineering - AIDIC;
653 2015. p. 2179-84.
654 [16] Steimke JL, Steeper TJ, Cólon-Mercado HR, Gorensek MB. Development and testing of a
655 PEM SO_2-depolarized electrolyzer and an operating method that prevents sulfur accumulation.
656 International Journal of Hydrogen Energy. 2015;40:13281-94.
657 [17] Niehoff AG, Botero NB, Acharya A, Thomey D, Roeb M, Sattler C, et al. Process
658 modelling and heat management of the solar hybrid sulfur cycle. International Journal of
659 Hydrogen Energy. 2015;40:4461-73.
660 [18] Lapp JL, Guerra-Niehoff A, Streber HP, Thomey D, Roeb M, Sattler C. Modeling of a solar
661 receiver for superheating sulfuric acid. American Society of Mechanical Engineers; 2015.
662 [19] Garrick TR, Gulledge A, Staser JA, Benicewicz B, Weidner JW. Polybenzimidazole
663 membranes for hydrogen production in the hybrid sulfur electrolyzer. In: Mustain WE, Brisard
664 G, Staser JA, Mogensen MB, Williams MC, Gur TM, et al., editors. Symposium on
665 Electrosynthesis of Fuels 3 - 227th ECS Meeting. 3 ed: Electrochemical Society Inc.; 2015. p.
666 31-40.
667 [20] Moore RC, Gelbard F, Parma EJ, Vernon ME, Lenard RX, Pickard PS. A Laboratory-Scale
668 Sulfuric Acid Decomposition Apparatus for Use in Hydrogen Production Cycles. Proceedings:
669 International Topical Meeting on Safety and Technology of Nuclear Hydr. 2007:161-6.
670 [21] Gorensek MB. Hybrid sulfur cycle flowsheets for hydrogen production using high-
671 temperature gas-cooled reactors. International Journal of Hydrogen Energy. 2011;36:12725-41.
672 [22] Gorensek MB, Summers WA. Hybrid sulfur flowsheets using PEM electrolysis and a
673 bayonet decomposition reactor. International Journal of Hydrogen Energy. 2009;34:4097-114.
674 [23] Guerra Niehoff A, Bayer Botero N, Acharya A, Thomey D, Roeb M, Sattler C, et al.
675 Process modelling and heat management of the solar hybrid sulfur cycle. International Journal of
676 Hydrogen Energy. 2015;40:4461-73.
677 [24] Kolb GJ, Diver RB, Siegel N. Central-Station Solar Hydrogen Power Plant. Journal of Solar
678 Energy Engineering. 2007;129:179-83.
679 [25] Ho CK, Iverson BD. Review of high-temperature central receiver designs for concentrating
680 solar power. Renewable and Sustainable Energy Reviews. 2014;29:835-46.
681 [26] Junginger R, Struck BD. Separators for electrolytic cells of the sulfuric acid hybrid cycle.
682 International Journal of Hydrogen Energy. 1982;7:331-40.
683 [27] Tang Z, Lawton JS, Sun C-N, Chen J, Bright MI, Jones AM, et al. Characterization of
684 Sulfonated Diels-Alder Poly(phenylene) Membranes for Electrolyte Separators in Vanadium
685 Redox Flow Batteries. Journal of the Electrochemical Society. 2014;161:A1860-A8.
686 [28] Park J. Sulfonated Perfluorocyclobutyl (PFCB) Aryl Ether Polymers: Synthesis, Reactivity,
687 and Characterization for Polymer Electrolyte Applications. All Dissertation: Clemson
688 University; 2013.
689 [29] Garrick TR, Wilkins CH, Pingitore AT, Gulledge A, Benicewicz B, Weidner JW.
690 Characterizing Voltage Losses in an SO_2 Depolarized Electrolyzer using Sulfonated
691 Polybenzimidazole Membranes. Journal of the Electrochemical Society. 2017;submitted for
692 publication.
693 [30] Ho C, Christian J, Gill D, Moya A, Jeter S, Abdel-Khalik S, et al. Technology
694 Advancements for Next Generation Falling Particle Receivers. Energy Procedia. 2014;49:398-
695 407.
696 [31] Ho CK. A review of high-temperature particle receivers for concentrating solar power.
697 Applied Thermal Engineering. 2016;109, Part B:958-69.

[32] Ho CK. Personal Communication. SNL is continuing work on the falling particle receiver ed2017.
[33] Sullivan SD, Kesseli J, Nash J, Farias J, Kesseli D, Caruso W. High-Efficiency Low-Cost Solar Receiver for Use In a Supercritical CO_2 Recompression Cycle. Brayton Energy, LLC, Portsmouth, NH (United States); 2016.
[34] Gorensek MB, Summers WA, Boltrunis CO, Lahoda EJ, Allen DT, Greyvenstein R. Hybrid Sulfur Process Reference Design and Cost Analysis. Savannah River National Laboratory, Aiken, SC, United States, 29808; 2009.
[35] Que H, Song Y, Chen C-C. Thermodynamic Modeling of the Sulfuric Acid−Water−Sulfur Trioxide System with the Symmetric Electrolyte NRTL Model. Journal of Chemical & Engineering Data. 2011;56:963-77.
[36] Gorensek M, Summers W, Boltrunis C, Lahoda E, Allen D, Greyvenstein R. Hybrid Sulfur Process Reference Design and Cost Analysis. 2009.
[37] Gorensek MB, Edwards TB. Energy Efficiency Limits for a Recuperative Bayonet Sulfuric Acid Decomposition Reactor for Sulfur Cycle Thermochemical Hydrogen Production. Industrial & Engineering Chemistry Research. 2009;48:7232-45.
[38] Gorensek MB, Staser JA, Stanford TG, Weidner JW. A thermodynamic analysis of the SO_2/H_2SO_4 system in SO_2-depolarized electrolysis. International Journal of Hydrogen Energy. 2009;34:6089-95.
[39] Wang P, Anderko A, Springer RD, Young RD. Modeling phase equilibria and speciation in mixed-solvent electrolyte systems: II. Liquid-liquid equilibria and properties of associating electrolyte solutions. Journal of Molecular Liquids. 2006;125:37-44.
[40] Kaur H, Gorensek MB, Chen C-C. Thermodynamic Modeling of the Hybrid Sulfur (HyS) Cycle for Hydrogen Production. Fluid Phase Equilibria. 2017;submitted for publication.
[41] US Department of Energy. SunShot Vision Study. 2012.
[42] Corgnale C, Summers WA. Solar hydrogen production by the Hybrid Sulfur process. Int J Hydrogen Energy. 2011;36:11604-19.
[43] Fuel Cell Technologies Office Multi-Year Research, Development, and Demonstration Plan, Section 3.1 Hydrogen Production. US Department of Energy; 2015.
[44] US Department of Energy. Concentrating Solar Power: Advanced Projects Offering Low LCOE Opportunities, CSP APOLLO, Modification 0002. 2015.

List of Figure Captions

Figure 1 The hybrid sulfur cycle.

Figure 2 SO_2-depolarized electrolysis section flowsheet.

Figure 3 High-temperature H_2SO_4 decomposition section flowsheet.

Figure 4 Composite heating and cooling curves for the high-temperature bayonet decomposition reactor for a 1-kmol/s hydrogen production rate (78.4 wt% H_2SO_4 feed at 278.9°C and 14.1 bar, 850°C peak fluid temperature, 650°C catalyst bed inlet temperature, 10°C minimum temperature difference).

Figure 5 Utility and grand composite curves for the high-temperature bayonet decomposition reactor for a 1-kmol/s hydrogen production rate.

Figure 6 Solar HyS flowsheet composite heating and cooling curves for a 1-kmol/s hydrogen production rate (10°C ΔT_{min}, bayonet reactor not included).

Figure 7 Solar HyS flowsheet utility and grand composite curves for a 1-kmol/s hydrogen production rate with steam heating.

Figure 8 Solar HyS flowsheet utility and grand composite curves for a 1-kmol/s hydrogen production rate with high-temperature helium heating.

Figure 9 Schematic of FPR solar plant with sand thermal energy storage coupled to a HyS process plant with pressurized helium heat transfer fluid

List of Table Captions

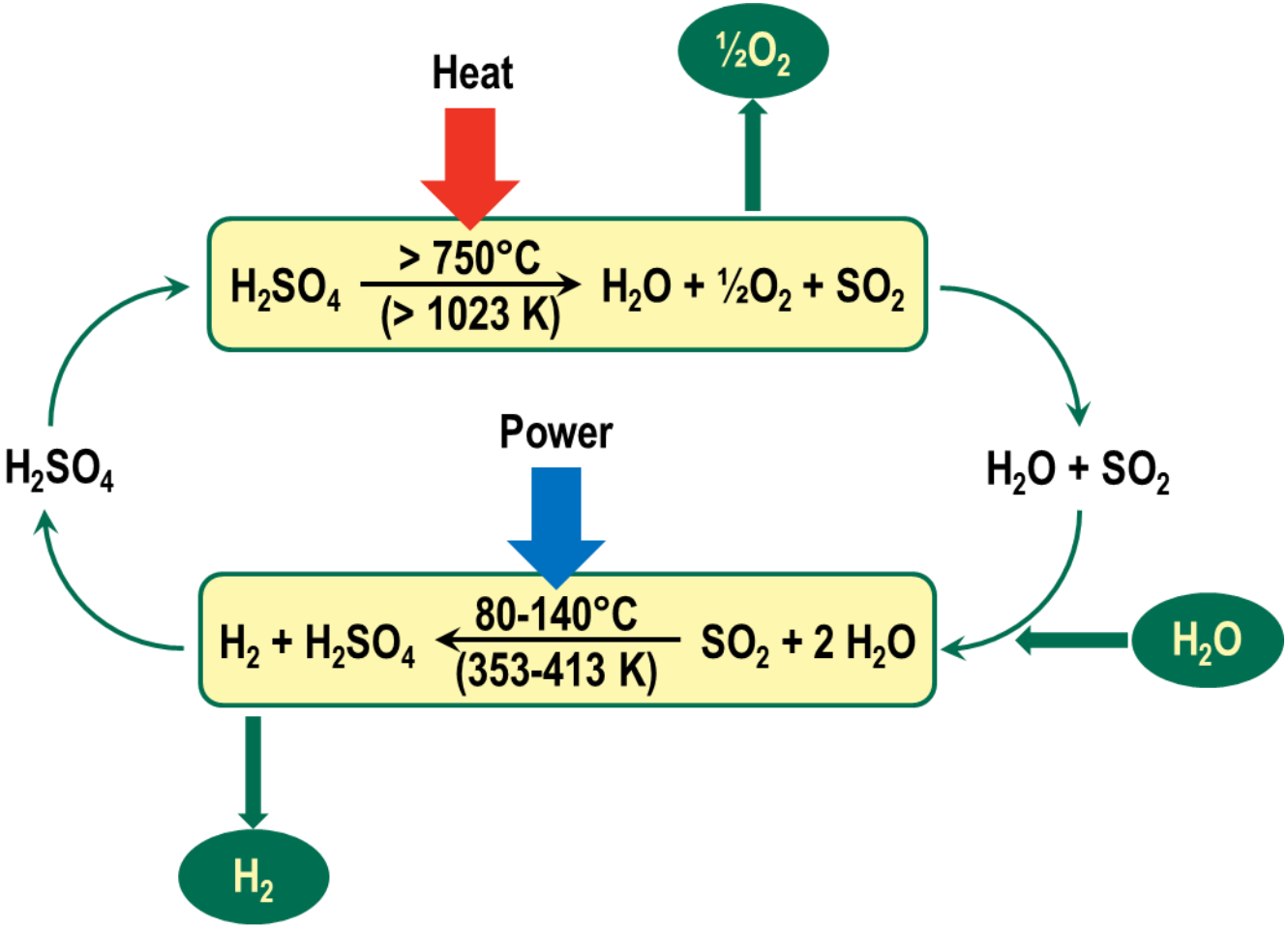
Heat
½O2
H2SO4
> 750°C
(> 1023 K)
H2O + ½O2 + SO2
Power
H2SO4
H2O + SO2
H2 + H2SO4
80-140°C
(353-413 K)
SO2 + 2 H2O
H2O
H2

Figure **1**

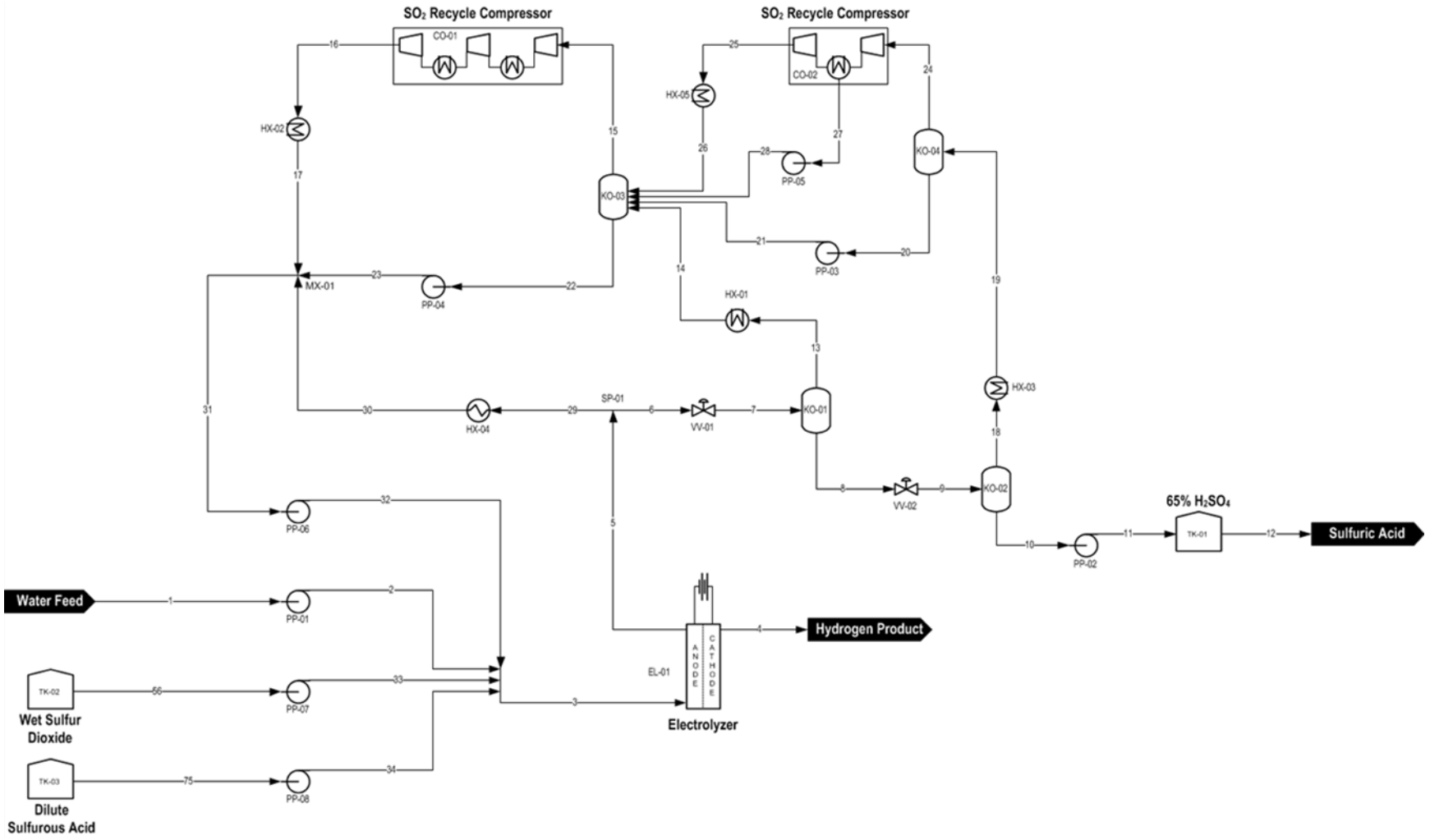
SO2 Recycle Compressor
SO2 Recycle Compressor
CO-01
CO-02
HX-05
HX-02
KO-04
PP-05
KO-03
PP-03
MX-01
PP-04
HX-01
HX-03
SP-01
HX-04
VV-01
KO-01
VV-02
KO-02
65% H2SO4
PP-06
PP-02
TK-01
Sulfuric Acid
Water Feed
PP-01
Hydrogen Product
EL-01
ANODE
CATHODE
TK-02
Wet Sulfur Dioxide
PP-07
TK-03
Dilute Sulfurous Acid
PP-08
Electrolyzer

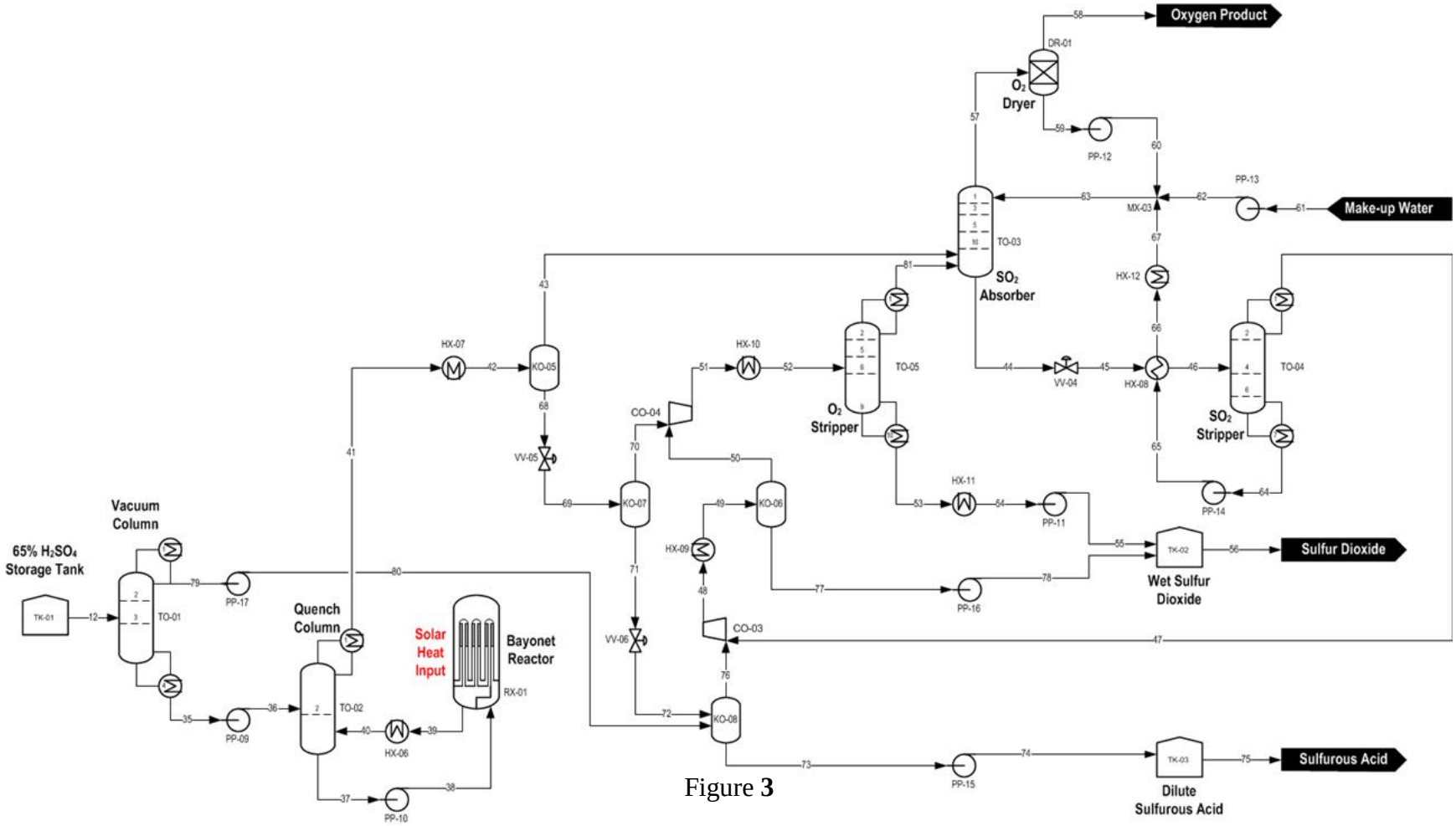
Oxygen Product
DR-01
O2 Dryer
PP-12
PP-13
Make-up Water
MX-03
TO-03
SO2 Absorber
HX-12
HX-07
KO-05
HX-10
TO-05
O2 Stripper
VV-04
HX-08
TO-04
SO2 Stripper
CO-04
VV-05
KO-07
KO-06
HX-11
PP-11
PP-14
HX-09
TK-02
Sulfur Dioxide
Wet Sulfur Dioxide
PP-16
CO-03
VV-06
Vacuum Column
65% H2SO4 Storage Tank
TK-01
TO-01
PP-17
Quench Column
Solar Heat Input
Bayonet Reactor
RX-01
TO-02
HX-06
PP-09
PP-10
KO-08
PP-15
TK-03
Sulfurous Acid
Dilute Sulfurous Acid

Figure **3**

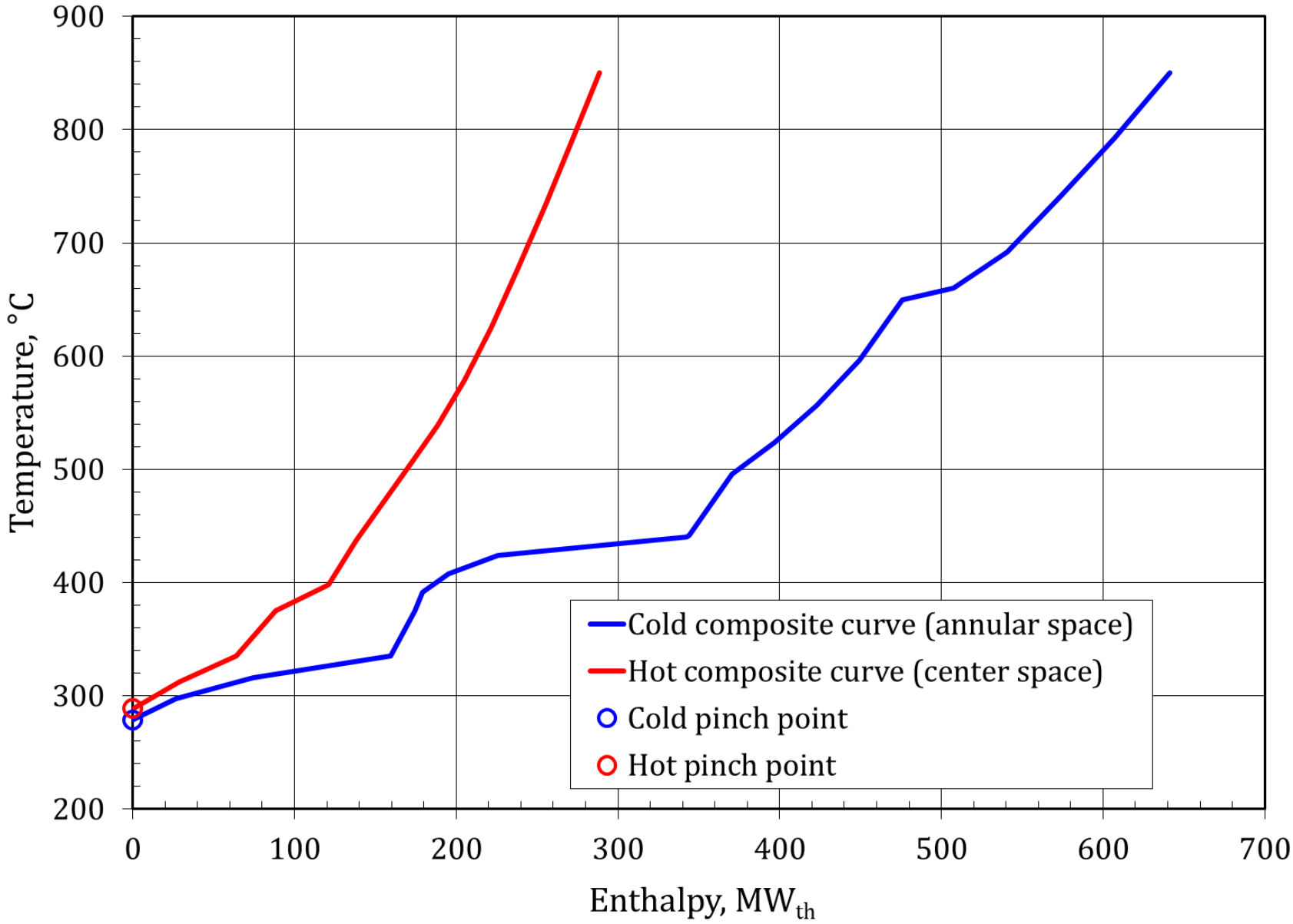
900
800
700
600
500
400
300
200
Temperature, °C
0
100
200
300
400
500
600
700
Enthalpy, MW$_{th}$
Cold composite curve (annular space)
Hot composite curve (center space)
Cold pinch point
Hot pinch point

Figure **4**

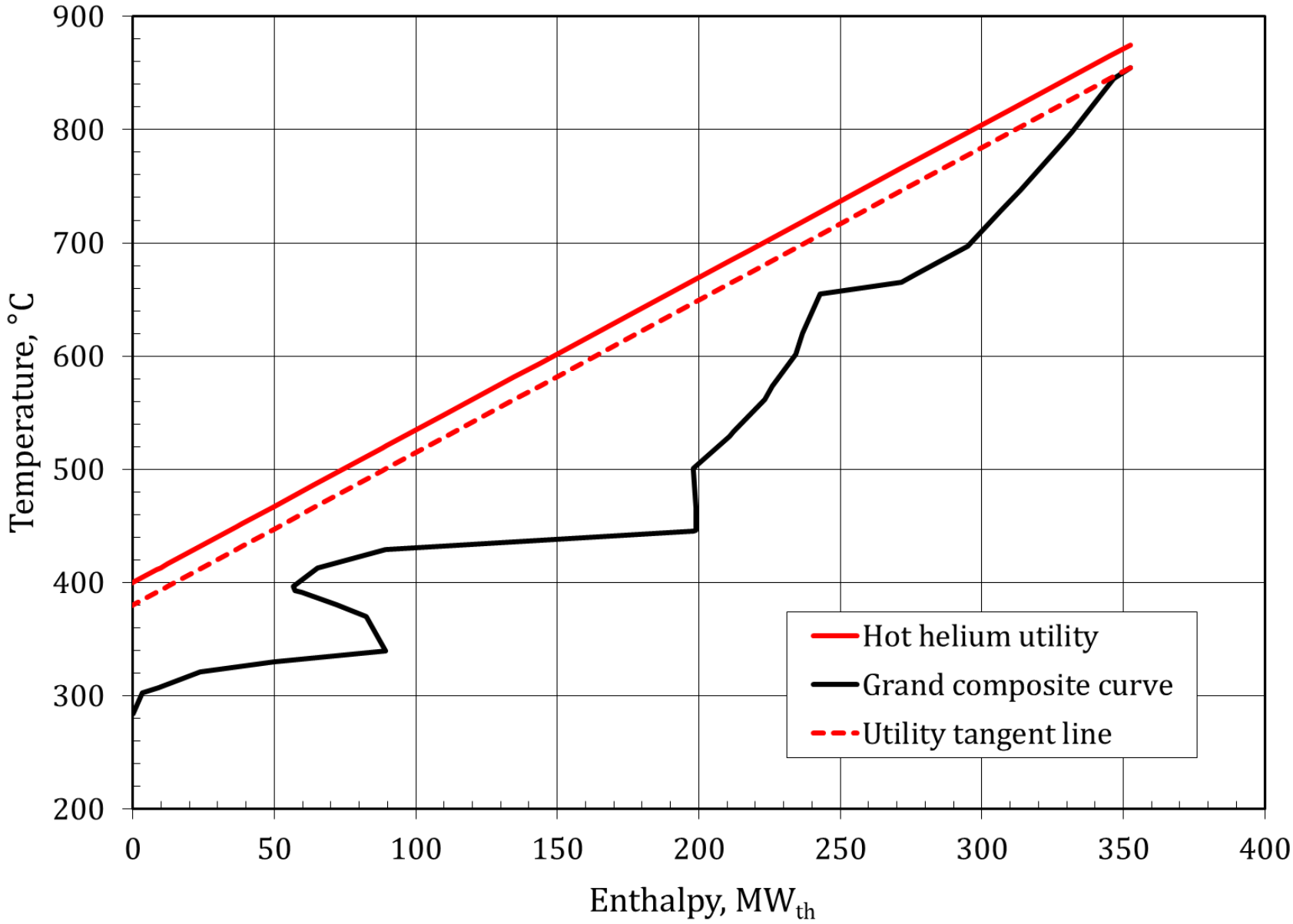
900
800
700
600
500
400
300
200
Temperature, °C
0
50
100
150
200
250
300
350
400
Enthalpy, MWth
Hot helium utility
Grand composite curve
Utility tangent line

Figure **5**

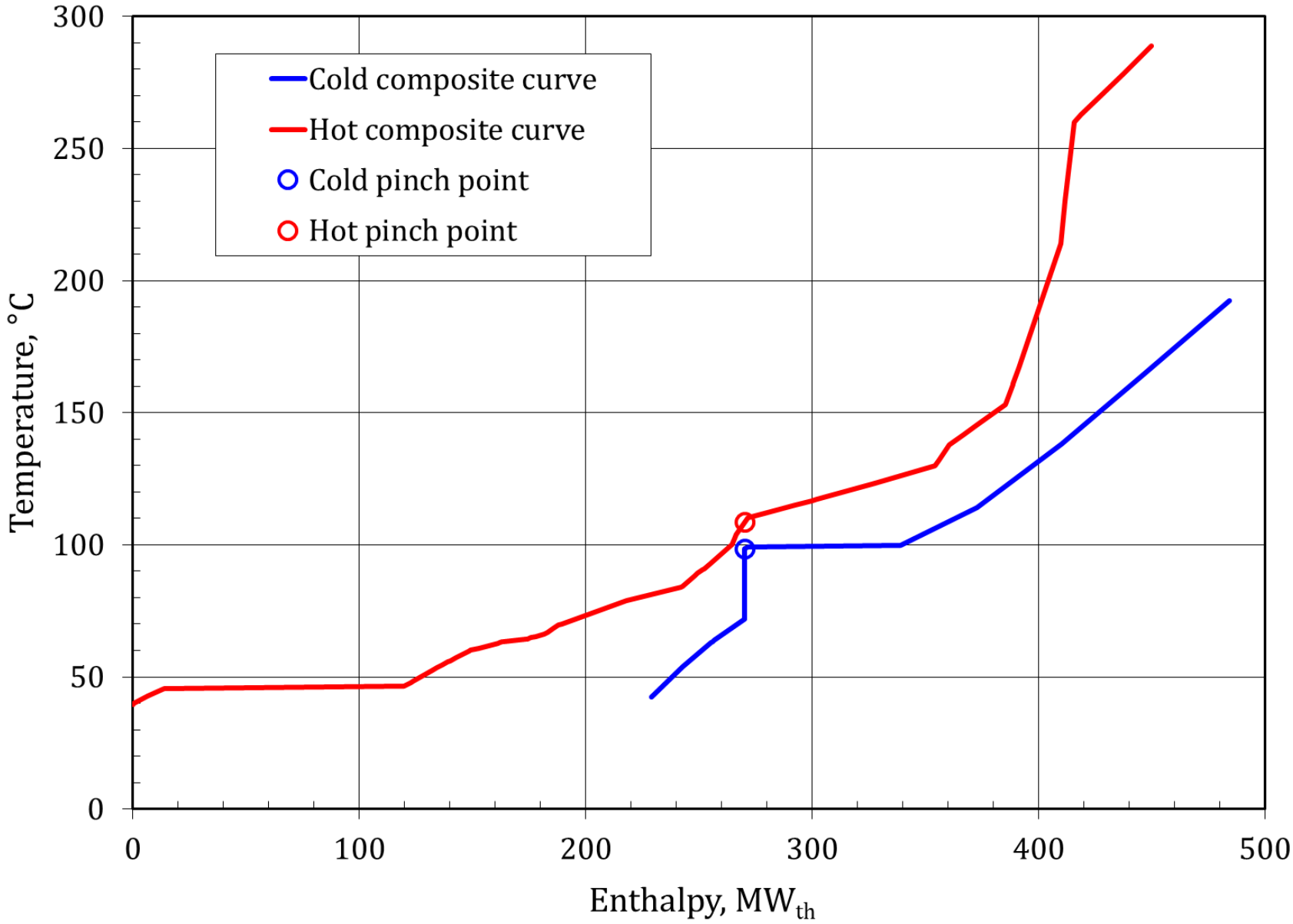
Cold composite curve
Hot composite curve
Cold pinch point
Hot pinch point
Temperature, °C
Enthalpy, MW$_{th}$
0
50
100
150
200
250
300
0
100
200
300
400
500

Figure **6**

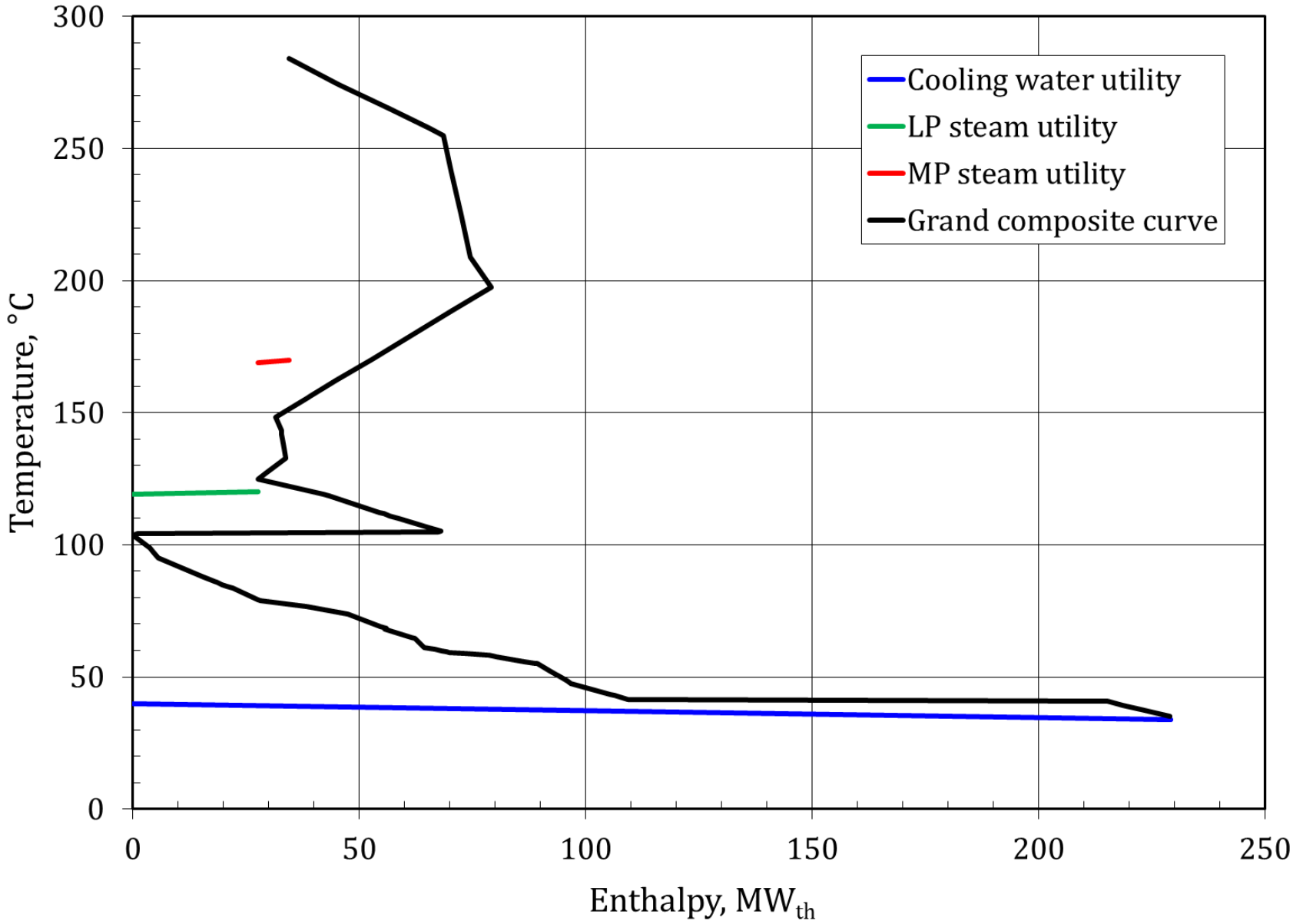
Cooling water utility
LP steam utility
MP steam utility
Grand composite curve
Temperature, °C
Enthalpy, MW$_{th}$
300
250
200
150
100
50
0
0
50
100
150
200
250

Figure **7**

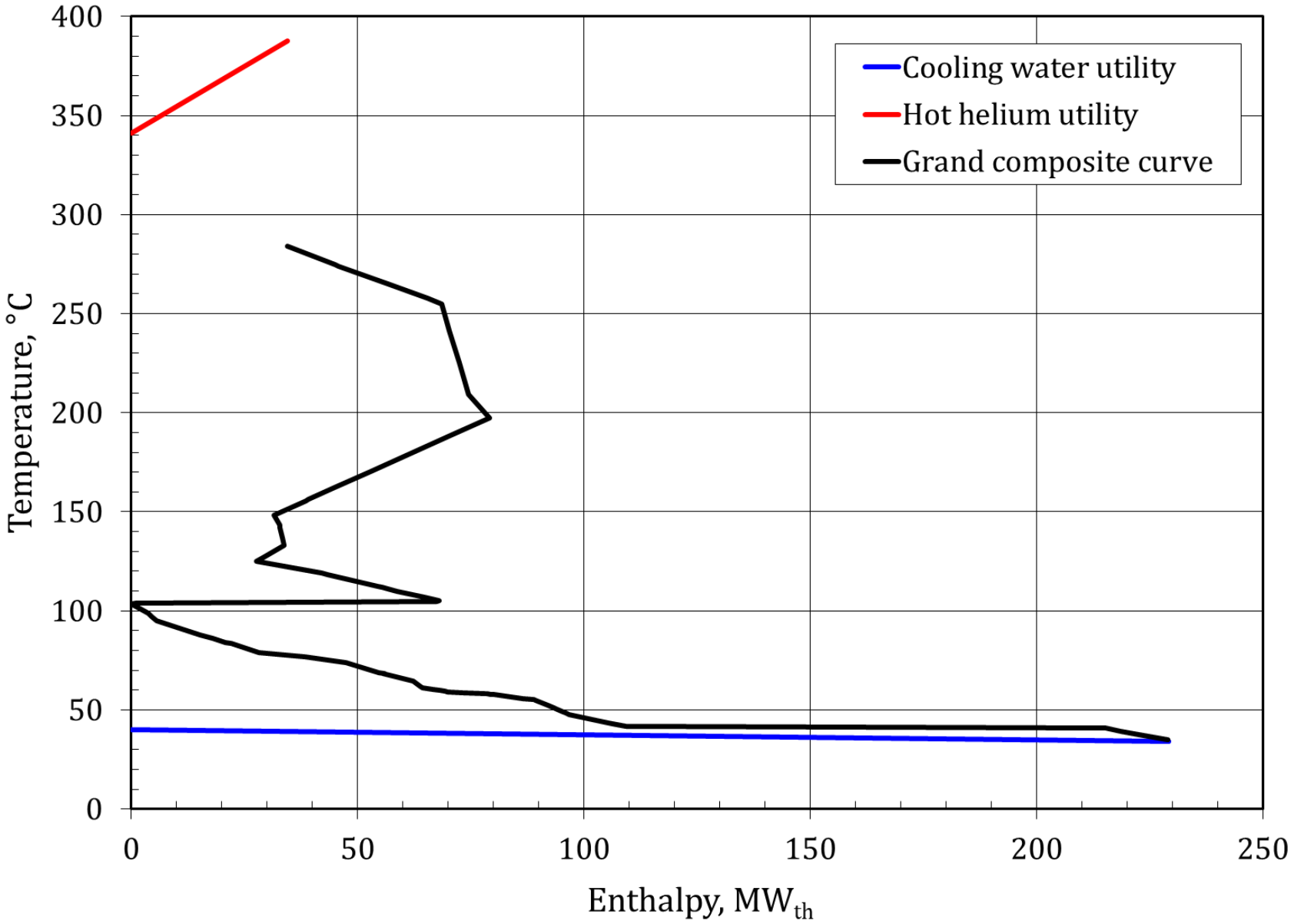
Cooling water utility
Hot helium utility
Grand composite curve
Temperature, °C
Enthalpy, MW$_{th}$
400
350
300
250
200
150
100
50
0
0
50
100
150
200
250

Figure **8**

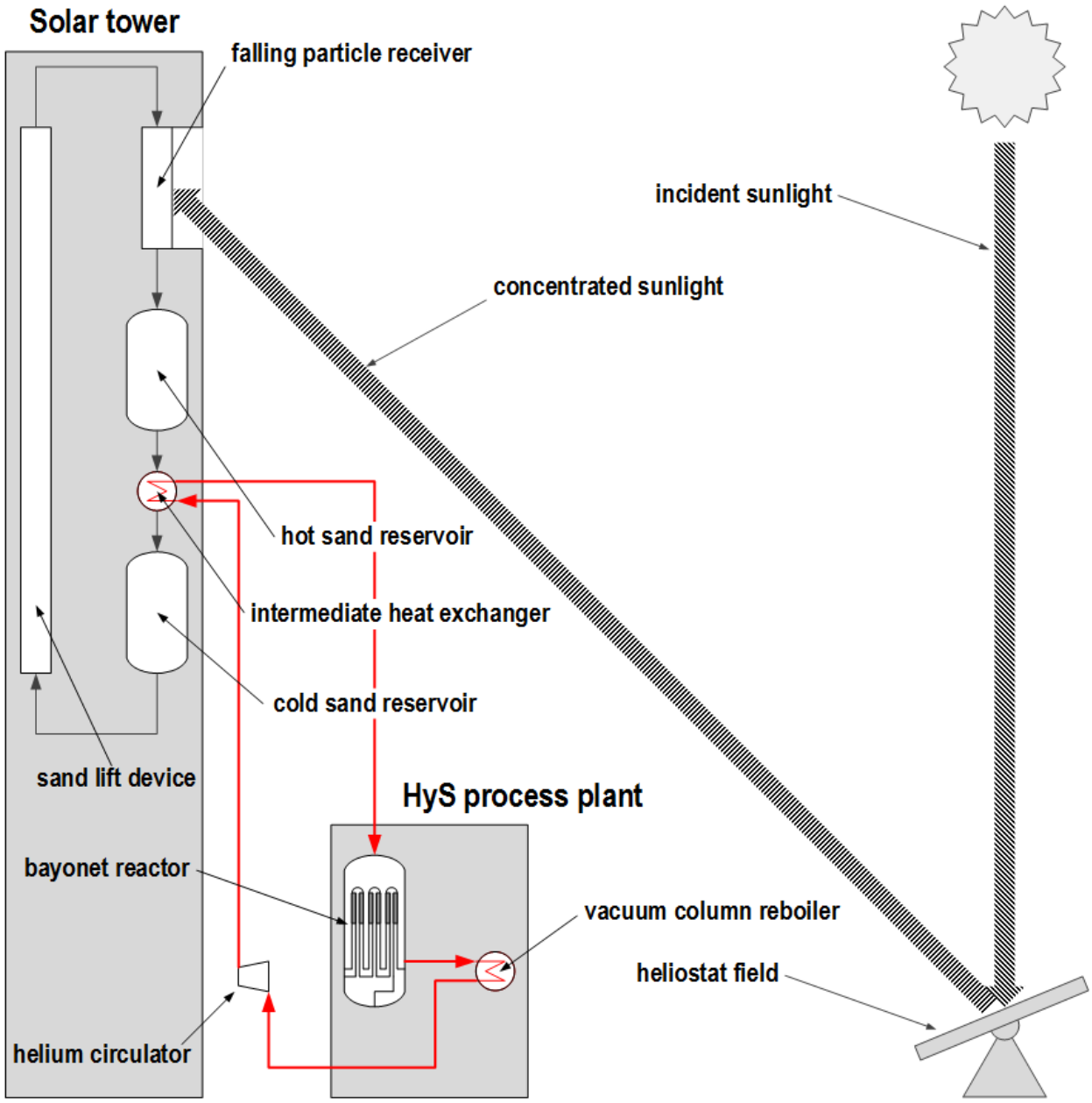
Solar tower
falling particle receiver
incident sunlight
concentrated sunlight
hot sand reservoir
intermediate heat exchanger
cold sand reservoir
sand lift device
HyS process plant
bayonet reactor
vacuum column reboiler
heliostat field
helium circulator

Figure **9**

Table 1

Stream	Molar flow rates, kmol/sec						Temperature,		Pressure,	Phase
ID	H_2O	H_2SO_4	SO_2	O_2	H_2	Total	°C	K	bar	
1	0.95993	0	0	0	0	0.95993	25.00	298.15	1.0000	L
2	0.95993	0	0	0	0	0.95993	25.80	298.95	22.700	L
3	52.129	15.336	2.0000	6.40E-09	0	69.465	114.79	387.94	22.700	L
4	0	0	0	0	1.0000	1.0000	130.00	403.15	21.700	V
5	50.129	16.336	1.0000	6.40E-09	0	67.465	130.00	403.15	21.700	L
6	3.0687	1.0000	0.061215	3.92E-10	0	4.1299	130.00	403.15	21.700	L
7	3.0687	1.0000	0.061215	3.92E-10	0	4.1299	117.22	390.37	1.0133	L + V
8	3.0453	1.0000	0.007551	2.00E-12	0	4.0529	117.22	390.37	1.0133	L
9	3.0453	1.0000	0.007551	2.00E-12	0	4.0529	91.59	364.74	0.10750	L + V
10	2.9312	1.0000	9.61E-05	6.19E-16	0	3.9313	91.59	364.74	0.10750	L
11	2.9312	1.0000	9.61E-05	6.19E-16	0	3.9313	91.61	364.76	1.0133	L
12	2.9312	1.0000	9.61E-05	6.19E-16	0	3.9313	91.61	364.76	1.0133	L
13	0.023356	5.97E-09	0.053664	3.90E-10	0	0.077020	117.22	390.37	1.0133	V
14	0.023356	5.97E-09	0.053664	3.90E-10	0	0.077020	40.00	313.15	0.91193	L + V
15	0.005631	7.23E-24	0.059626	3.92E-10	0	0.065257	41.28	314.43	0.91193	V
16	0.005631	7.23E-24	0.059626	3.92E-10	0	0.065257	193.49	466.64	21.200	V
17	0.005631	7.23E-24	0.059626	3.92E-10	0	0.065257	40.00	313.15	21.000	L
18	0.11410	1.17E-08	0.007455	2.00E-12	0	0.12155	91.59	364.74	0.10750	V
19	0.11410	1.17E-08	0.007455	2.00E-12	0	0.12155	40.00	313.15	0.09675	L + V
20	0.090347	1.17E-08	5.28E-05	1.03E-17	0	0.090400	40.00	313.15	0.09675	L
21	0.090347	1.17E-08	5.28E-05	1.03E-17	0	0.090400	40.06	313.21	0.91193	L
22	0.13182	1.76E-08	0.001493	1.35E-14	0	0.13332	41.28	314.43	0.91193	L
23	0.13182	1.76E-08	0.001493	1.35E-14	0	0.13332	42.49	315.64	21.000	L
24	0.023751	1.73E-24	0.007402	2.00E-12	0	0.031153	40.00	313.15	0.09675	V
25	0.002416	1.73E-24	0.007326	2.00E-12	0	0.009742	146.77	419.92	1.0133	V
26	0.002416	1.73E-24	0.007326	2.00E-12	0	0.009742	40.00	313.15	0.91193	L + V
27	0.021335	0	7.57E-05	0	0	0.021411	40.00	313.15	0.29700	L
28	0.021335	0	7.57E-05	0	0	0.021411	40.05	313.20	0.91193	L
29	47.061	15.336	0.93879	6.01E-09	0	63.336	130.00	403.15	21.700	L
30	47.061	15.336	0.93879	6.01E-09	0	63.336	110.13	383.28	21.000	L
31	47.183	15.336	0.99990	0	0	63.519	110.35	383.50	21.000	L
32	47.183	15.336	0.99990	0	0	63.519	110.46	383.61	22.700	L
33	0.069287	0	0.92987	6.14E-09	0	0.99916	35.48	308.63	22.700	L
34	3.9175	8.38E-06	0.070225	2.63E-10	0	3.9878	26.89	300.04	22.700	L
56	0.069287	0	0.92987	6.14E-09	0	0.99916	34.97	308.12	12.000	L
75	3.9175	8.38E-06	0.070225	2.63E-10	0	3.9878	26.25	299.40	2.0000	L

Table 2

Stream	Molar flow rates, kmol/sec						Temperature,		Pressure,	Phase
ID	H_2O	H_2SO_4	SO_2	O_2	H_2	Total	°C	K	bar	
12	2.9312	1.0000	9.61E-05	0	0	3.9313	91.61	364.76	1.0133	L
35	0.60492	1.0000	7.79E-15	0	0	1.6049	192.44	465.59	0.11500	L
36	0.60492	1.0000	2.45E-13	0	0	1.6049	192.90	466.05	12.500	L
37	2.3180	1.5445	0.022865	0.000310	0	3.8857	278.91	552.06	12.500	L
38	2.3180	1.5445	0.022865	0.000310	0	3.8857	278.93	552.08	14.100	L
39	3.3180	0.54454	1.0229	0.50031	0	5.3857	288.93	562.08	13.100	L + V
40	3.3180	0.54454	1.0229	0.50031	0	5.3857	260.00	533.15	12.500	L + V
41	1.6049	8.38E-06	1	0.50000	0	3.1049	214.00	487.15	12.500	V
42	1.6049	8.38E-06	1	0.50000	0	3.1049	40.00	313.15	12.000	L + V
43	0.007494	2.17E-21	0.68625	0.49973	0	1.1935	40.00	313.15	12.000	V
44	11.364	0	0.69338	0.001297	0	12.059	56.67	329.82	12.000	L
45	11.364	0	0.69338	0.001297	0	12.059	42.55	315.70	1.2133	L + V
46	11.364	0	0.69338	0.001297	0	12.059	71.76	344.91	1.0133	L + V
47	0.063112	0	0.69327	0.001297	0	0.75768	39.59	312.74	0.86325	V
48	0.068308	1.30E-23	0.82103	0.001298	0	0.89064	161.18	434.33	3.6870	V
49	0.068308	1.30E-23	0.82103	0.001298	0	0.89064	40.00	313.15	3.4870	L + V
50	0.017527	0	0.81825	0.001298	0	0.83708	40.00	313.15	3.4870	V
51	0.018507	1.41E-23	0.93411	0.00157	0	0.95419	145.12	418.27	12.311	V
52	0.018507	1.41E-23	0.93411	0.00157	0	0.95419	60.00	333.15	12.111	L + V
53	0.018507	0	0.92709	5.25E-16	0	0.94560	63.26	336.41	12.200	L
54	0.018507	0	0.92709	5.25E-16	0	0.94560	40.00	313.15	11.900	L
55	0.018507	0	0.92709	5.25E-16	0	0.94560	40.00	313.15	12.000	L
56	0.069287	0	0.92987	6.14E-09	0	0.99916	34.97	308.12	12.000	L
57	0.003386	0	1.13E-06	0.50000	0	0.50339	40.03	313.18	11.800	V
58	0	0	0	0.50000	0	0.50000	40.03	313.18	11.000	V
59	0.003386	0	1.13E-06	0	0	0.003387	40.03	313.18	11.000	L
60	0.003386	0	1.13E-06	0	0	0.003387	40.09	313.24	11.800	L
61	0.055618	0	0	0	0	0.055618	40.00	313.15	1.0000	L
62	0.055618	0	0	0	0	0.055618	40.88	314.03	11.800	L
63	11.360	0	0.000116	5.17E-23	0	11.360	40.00	313.15	11.800	L
64	11.301	0	0.000115	5.17E-23	0	11.301	99.80	372.95	1.01325	L
65	11.301	0	0.000115	5.17E-23	0	11.301	100.13	373.28	12.200	L
66	11.301	0	0.000115	5.17E-23	0	11.301	52.55	325.70	12.000	L
67	11.301	0	0.000115	5.17E-23	0	11.301	40.00	313.15	11.800	L
68	1.5974	8.38E-06	0.31375	0.000273	0	1.9115	40.00	313.15	12.000	L
69	1.5974	8.38E-06	0.31375	0.000273	0	1.9115	24.35	297.50	3.4870	L + V
70	0.000980	1.41E-23	0.11586	0.000272	0	0.11711	24.35	297.50	3.4870	V
71	1.5964	8.38E-06	0.19789	4.46E-07	0	1.7943	24.35	297.50	3.4870	L
72	1.5964	8.38E-06	0.19789	4.46E-07	0	1.7943	3.28	276.43	0.86325	L + V
73	3.9175	8.38E-06	0.070225	2.63E-10	0	3.9878	26.22	299.37	0.86325	L
74	3.9175	8.38E-06	0.070225	2.63E-10	0	3.9878	26.25	299.40	2.0000	L

75	3.9175	8.38E-06	0.070225	2.63E-10	0	3.9878	26.25	299.40	2.0000	L
76	0.005196	1.30E-23	0.12776	4.46E-07	0	0.13296	26.22	299.37	0.86325	V
77	0.050781	0	0.002778	6.14E-09	0	0.053558	40.00	313.15	3.4870	L
78	0.050781	0	0.002778	6.14E-09	0	0.053558	40.71	313.86	12.000	L
79	2.3263	2.75E-21	9.61E-05	0	0	2.3264	45.74	318.89	0.10000	L
80	2.3263	0	9.61E-05	0	0	2.3264	45.76	318.91	0.86325	L
81	8.28E-08	0	0.007018	0.001570	0	0.008588	53.41	326.56	12.000	V

Table 3

Unit ID	Description	Power, MW_e
EL-01	SO_2-depolarized electrolyzer	115.8
CO-01A	Low-pressure SO_2 recycle compressor, 1st stage	0.2411
CO-01B	Low-pressure SO_2 recycle compressor, 2nd stage	0.2581
CO-01C	Low-pressure SO_2 recycle compressor, third stage	0.2624
CO-02A	High-pressure SO_2 recycle compressor, 1st stage	0.1354
CO-02B	High-pressure SO_2 recycle compressor, 2nd stage	0.04162
CO-03	1st Stage SO_2 recycle compressor	4.517
CO-04	2nd Stage SO_2 recycle compressor	3.978
PP-01	Water feed pump	0.05751
PP-02	Acid product pump	0.01064
PP-03	2nd Flash stage condensate pump	0.000395
PP-04	1st Flash stage condensate pump	0.01230
PP-05	HP SO_2 recycle compressor intercooler condensate pump	0.000081
PP-06	Anolyte recycle pump	0.3078
PP-07	Wet SO_2 feed pump	0.06577
PP-08	Dilute sulfurous acid feed pump	0.1964
PP-09	Vacuum column bottoms pump	0.1083
PP-10	Quench column bottoms pump	0.02785
PP-11	O_2 stripper bottoms pump	0.000608
PP-12	O_2 dryer liquids pump	0.000017
PP-13	SO_2 absorber make-up water feed pump	0.003688
PP-14	SO_2 stripper bottoms pump	0.2818
PP-15	Dilute sulfurous acid pump	0.01079
PP-16	1st Stage SO_2 recycle compressor effluent condensate pump	0.003049
PP-17	Vacuum column distillate pump	0.004373
	Total power requirement	126.3

Table 4

Unit ID	Description	Duty, MW_{th}	Temperature, °C	
			Inlet	Outlet
RX-01	High-temperature bayonet decomposition reactor	352.6	278.9	288.9
TO-01R	Vacuum column reboiler	148.4	98.5	192.4
TO-04R	SO_2 stripper reboiler	65.55	99.1	99.8
HX-08	SO_2 stripper feed/bottoms interchanger, cold side	40.59	42.5	71.8
TO-05R	O_2 stripper reboiler	0.6036	63.2	63.3
	Total heat duty	607.8		

Table 5

Unit ID	Description	Duty, MW_{th}	Temperature, °C	
			Inlet	Outlet
CO-01-H1	Low-pressure SO_2 recycle compressor stage 1-2 intercooler	0.1717	132.2	70.0
CO-01-H2	Low-pressure SO_2 recycle compressor stage 2-3 intercooler	0.2226	167.1	90.0
CO-02-H	High-pressure SO_2 recycle compressor intercooler	1.063	160.7	40.0
DR-01	O_2 dryer	0.1423	40.0	40.0
HX-01	1st Flash stage vapor cooler	1.050	117.2	40.0
HX-02	High-pressure SO_2 recycle compressor discharge cooler	1.906	193.5	40.0
HX-03	2nd Flash stage vapor cooler	2.576	90.7	40.0
HX-04	Anolyte recycle cooler	66.72	130.0	110.1
HX-05	Low-pressure SO_2 recycle compressor discharge cooler	0.1195	146.8	40.0
HX-06	Bayonet reactor effluent cooler	31.28	288.9	260.0
HX-07	Quench column overhead cooler	95.40	214.0	40.0
HX-08	SO_2 stripper feed/bottoms interchanger, hot side	40.59	100.1	52.5
HX-09	1st Stage SO_2 recycle compressor discharge cooler	6.867	161.2	40.0
HX-10	2nd Stage SO_2 recycle compressor discharge cooler	22.95	145.1	60.0
HX-11	O_2 stripper bottoms product cooler	2.319	62.9	40.0
HX-12	SO_2 absorber water feed cooler	10.67	52.5	40.0
TO-01C	Vacuum column condenser	104.4	46.5	45.7
TO-02C	Quench column condenser	8.700	278.9	214.0
TO-04C	SO_2 stripper condenser	52.13	83.9	39.6
TO-05C	O_2 stripper condenser	0.5853	60.1	53.4
	Total cooling duty	449.9		

Table 6

Item	Value	Comments
Solar multiple	2.7	Based on typical weather for the southwest US desert [41]
Plant capacity factor (PCF), %	75	Based on the solar multiple and presence of TES
Heliostat efficiency, %	55	Based on SunShot Initiative goals, accounting for all inefficiencies (i.e., heliostat optical efficiency, cosine losses, atmospheric attenuation, etc.) and on [42]
Receiver efficiency, %	91	Based on SunShot Initiative goals [41] and on currently achievable values
TES energy efficiency, %	99	Based on SunShot Initiative goals [44]
Power cycle efficiency, %	41.6	Based on SunShot Initiative goals [41]
Solar-to-electric efficiency, %	20.6	Based on the power cycle efficiency value and the SunShot Initiative goals [41]

Table 7

Item	Value
Heat transfer fluid	Pressurized helium
Operating pressure, bar	40
Intermediate heat transfer loop total pressure drop, bar	1.2

Table 8

Unit (see Figure 9)	Duty, MW	Comments
Intermediate heat transfer loop	–	He flow rate = 144.5 kg/s Operating pressure = 40 bar Maximum/minimum temperature = 875/354°C Total pressure drop = 1.2 bar
Bayonet reactor	352.6	Helium supply temperature = 875°C Helium return temperature = 400°C
Vacuum column reboiler	34.6	External heat for vacuum column reboiler Helium supply temperature = 400°C Helium return temperature = 354°C
He circulator	10.4	Electric power Helium inlet temperature = 354°C Helium outlet temperature = 367°C
HyS process plant power requirement	126.3	Electric power required by the HyS process plant (W_{TC}), from Table **3**
Intermediate heat exchanger	376.8	Helium inlet temperature = 367°C Helium outlet temperature = 875°C
FPR heat input	418.7	Receiver heat input, with receiver + TES efficiency = 90%
Heliostat field solar heat input	761.3	Heliostat field heat input (Q_H), with heliostat efficiency = 55% Peak solar heat input = 2055.4 MW_{th}